MCMASTER UNIVERSITY
FACULTY OF SCIENCE
Department of Mathematics and Statistics

Soliton Interactions with Dispersive Wave Background

A Thesis Submitted in Partial Fulfillment of the Requirements for the Master of Science Degree

by

Ana Mucalica

Bachelor of Science in Mathematics
Department of Mathematics and Statistics
Faculty of Science, McMaster University, 2023

Supervised By

Dr. Dmitry Pelinovsky

Hamilton, 2023

Abstract

The Korteweg – de Vries (KdV) equation is a classical model for describing long surface gravity waves propagating in dispersive media. It is known to possess many families of exact analytic solutions, including solitons, which due to their distinct physical nature, are of particular interest to physicists and mathematicians alike. The propagation of solitons on the background of large-scale waves is a fundamental problem, with applications in fluid dynamics, nonlinear optics and condensed matter physics. This thesis centers around construction and analysis of a soliton as it interacts with either a rarefaction wave (RW) or a modulated dispersive shock wave. Using the Darboux transformation for the KdV equation, we construct and analyze exact solutions describing the dynamic interaction of a soliton and a dispersive mean field.

Dedication

I dedicate this thesis to my family, for their continuous love and support.

Acknowledgment

I would like to take this opportunity to express my sincerest gratitude towards my supervisor Dr. Dimitry Pelinovsky, who introduced me to the fascinating soliton theory with much rigor and passion. I am very grateful for his support and understanding throughout the duration of my graduate studies.

I would also like to thank my peers at McMaster University for their friendship, their continuous encouragement, and many important (and of course, unimportant) mathematical discussions.

This research was generously supported by my supervisor and the Department of Mathematics at McMaster University.

Contents

List of Figures

Introduction

A soliton is a spatially localized traveling wave solution of nonlinear partial differential equations (PDEs) which results from an optimal balance of dispersive and nonlinear effects. Since their discovery in 1834, solitons continue to fascinate both physicists and mathematicians alike. They arise in the context of fluid dynamics, nonlinear optics, and condensed matter physics.

Mathematically, solitons arise as solutions of nonlinear wave equations that are exactly solvable by the inverse scattering transform (IST) method. The integrability, coupled with the physical relevance of these structures, has led to the construction and analysis of various soliton interaction solutions for a wide range of wave equations, of which a benchmark model is known as the Korteweg–de Vries (KdV) equation.

Traditionally, the KdV equation has mostly been studied on spatial domains with decaying boundary conditions, and resulting $N-$soliton interactions on a trivial, zero background is a well-understood problem. In recent years however, motivated by developments of available algebraic tools used to study such nonlinear PDEs, as well as advancements in physical experimental design, researchers have been actively tackling more complicated interaction patterns between solitons and dispersive waves.

Applications of such interaction patterns are broad ranging. In fact, wherever the fundamental processes of dispersive hydrodynamics arise, e.g. in geophysical fluid dynamics (tidal bores, earthquake generated waves, etc.) or photonic waves (telecommunications), solitons and dispersive wave interactions can occur.

In this thesis, we focus on the Kortewed–de Vries equation, which we use to construct and analyze a soliton as it interacts with rarefaction waves (RW) or modulated dispersive shock waves (DSW). As an alternative to the more traditional IST method, we use Darboux transformation to construct and analyze these exact solutions describing the interaction of a solitary wave and a dispersive mean field.

The thesis is organized as follows.

The Korteweg–de Vries equation, along with the main motivation for this thesis is introduced in Section 1.1 of the first Chapter. In Section 1.2, we present a brief overview of the IST method and a linear Lax pair which define the spectral problem. Finally, Chapter 1 concludes with an outline of the Darboux transformation and a simple application of one soliton on the zero background.

In Chapter 2 we construct a soliton on the rarefaction wave background and present two different types of interactions depending on the soliton amplitude. Numerical analysis of our findings is presented at the end of Chapter 2.

Two family of solutions asscoiated with soliton-periodic cnoidal wave interactions are constructed in Chapter 3. The properties and characterization of both solution families is presented in Sections 3.5 and 3.6.

The thesis is concluded with Chapter 4, which contains remarks and open problems.

It is worth mentioning that Chapter 2 is based on a published paper [39], and Chapter 3 is based on an accepted paper [28].

Chapter 1

Background and Motivation

1.1 Kortewed–de Vries Equation

The Korteweg–de Vries (KdV) equation is a classical model for long surface gravity waves of small amplitude propagating over the shallow water of uniform depth. The normalized version of the KdV equation takes the form

$$u_t + 6uu_x + u_{xxx} = 0, \tag{1.1}$$

where t is the evolution time, x is the spatial coordinate for the wave propagation, and u is the fluid velocity. The KdV equation has predominantly been studied on spatial domains with either decaying or periodic boundary conditions.

Due to the complete integrability of the KdV equation, soliton interactions under decaying conditions, can be described by the exact N-soliton solutions, which can be constructed by successive Darboux transformations [35]. Darboux transformations achieve a nonlinear superposition principle by effectively "adding" one soliton to the solution.

However, more recently, different classes of solutions of the KdV equation have been identified, for which a localized soliton interacts with the dynamical field. The purpose of this thesis is to use the Darboux transformation and obtain the nonlinear superposition of a single soliton and a dispersive wave background. Depending on the nature of these interactions, the characterization of the exact solutions is either done analytically, by explicitly plotting parameters that define the interaction solution or numerically, by using a finite difference scheme for the KdV equation.

The motivation for this study comes from recent experiments that explore the interaction of solitons and dispersive mean fields [4, 36, 44].

Maiden et. al [36] recently used the Whitham modulation theory which is an approximate method for studying modulated nonlinear wavetrains, to study solitary waves, interacting with either rarefaction wave (RW) or a dispersive shock wave (DSW). In both cases, two different scenarios emerge. Either the solitary wave incident upon the mean field tunnels through the mean field to then propagate freely on the other side with an altered amplitude and speed. Or, the incident solitary wave remains trapped within the interior of the mean field, as depicted in Figure 1.1 below. This paper, along with works of [1] motivated our discussion on soliton - rarefaction wave interaction presented in Chapter 2. A detailed overview of the soliton-mean field interaction was recently presented in [4], and is in full agreement with our findings.

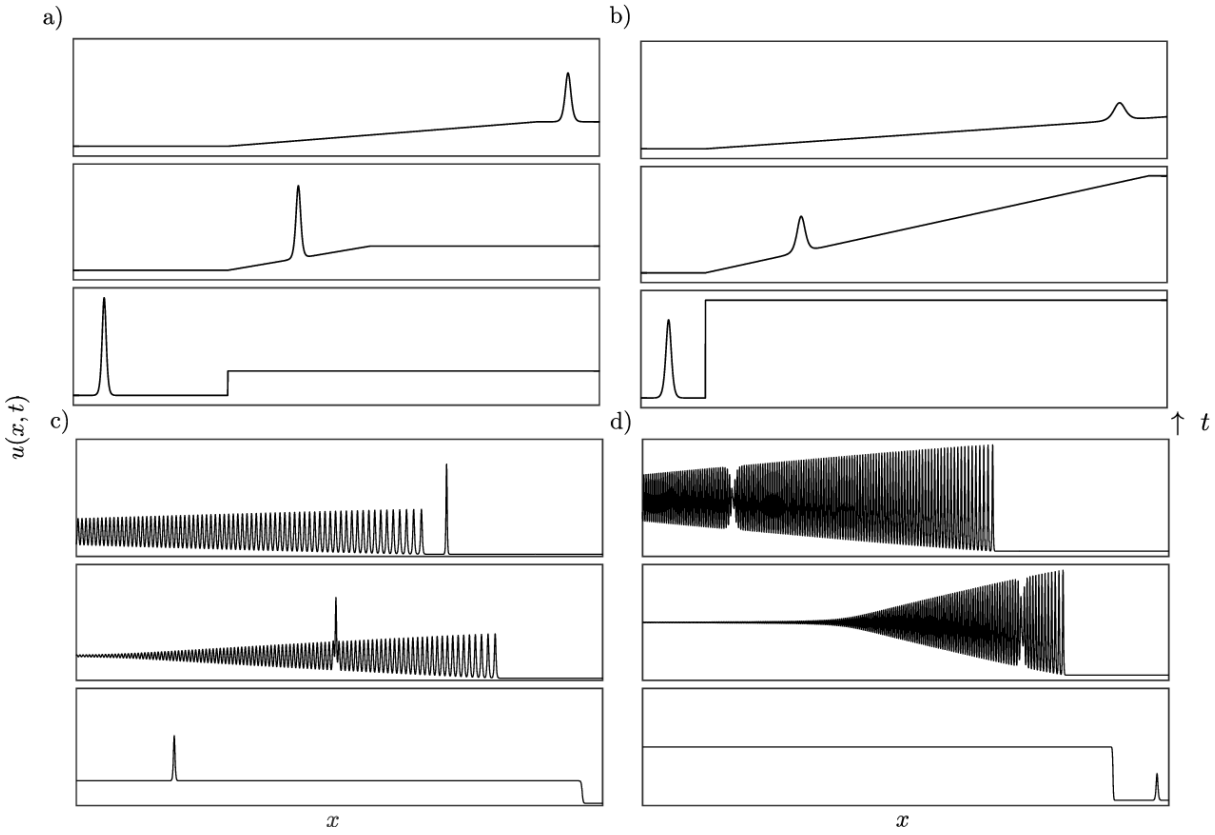

FIGURE 1.1: Soliton-mean field interaction scenarios taken from [4]. a) Soliton-RW tunneling. b) Soliton-RW trapping. c) Soliton-DSW tunneling. d) Soliton-DSW trapping.

The motivation for the construction of the soliton-cnoidal wave interactions discussed in Chapter 3, comes from the fact that the DSWs can be also viewed as modulated cnoidal waves, [20, 21] and the soliton-DSW interaction is analogous to the soliton-cnoidal wave

interaction. Two different types of soliton-DSW interaction dynamics were observed in [36], and are shown at the bottom (c-d) of Figure 1.1. When a soliton completely passes through a DSW, the nature of the interaction gives rise to an elevation (bright) nonlinear wavepacket. On the other hand, when a soliton becomes embedded or trapped within a DSW, the trapped soliton resembles a depression (dark) nonlinear wavepacket.

The exact solutions for the soliton-cnoidal wave interactions have previously been constructed using other solution methods. The first work was developed in [31] within the stability analysis of a cnoidal wave of the KdV equation. The authors used the Marchenko equation of the inverse scattering transform and obtained exact solutions for the "dislocations" of the cnoidal wave. More special solutions for the soliton-cnoidal wave interactions were obtained in [29] by using the nonlocal symmetries of the KdV equation. These solutions are expressed in a closed form as integrals of Jacobi elliptic functions, but they do not represent the most general exact solutions for the soliton-cnoidal wave interactions.

A related problem on a soliton interacting with a nonlinear wavetrain that asymptotes to a cnoidal wave was studied in [5, 25]. This soliton-mean field problem is equivalent to a test soliton propagating through a soliton condensate, a special kind of soliton gas [14], linking soliton-mean interaction to breather solutions, which play an important role in soliton-DSW interaction.

1.2 Inverse Scattering Transform and the Lax Pair

What generated interest in the soliton theory since the second half of the 1900s was the discovery of the Inverse Scattering Transform, or IST for short, and its generalization to a large class of nonlinear wave equations. This method is remarkable because it allows us to solve the initial-value problem for nonlinear PDEs exactly.

The initial value problem for the KdV equation can be analyzed by means of the IST method [41], by relating a solution of the KdV equation (1.1) to the spectrum of the stationary Schrödinger equation

$$\mathcal{L}v = \lambda v, \qquad \mathcal{L} := -\frac{\partial^2}{\partial x^2} - u \tag{1.2}$$

and the time-evolution equation

$$\frac{\partial v}{\partial t} = \mathcal{M}v, \qquad \mathcal{M} := -3u_x - 6u\frac{\partial}{\partial x} - 4\frac{\partial^3}{\partial x^3}. \tag{1.3}$$

where λ is the time-independent spectral parameter. The above equations (1.2), (1.3) form the linear Lax pair, and the values of λ are independent of (x,t) if $\mathcal{L}$ and $\mathcal{M}$ satisfy the compatibility condition

$$\frac{\partial \mathcal{L}}{\partial t} + \mathcal{L}\mathcal{M} = \mathcal{M}\mathcal{L} \tag{1.4}$$

which yields the KdV equation (1.1) for $u = u(x,t)$.

In the case of the KdV equation, solving the linear problem (1.2) is equivalent to finding the eigenvalues and the corresponding eigenfunctions of $\mathcal{L}$. The eigenvalues and the behaviour of the eigenfunctions as $|x| \to \infty$ determine the scattering data at any time t.

The overview of the IST scheme for the KdV equation (1.1) is shown in figure 1.2 below.

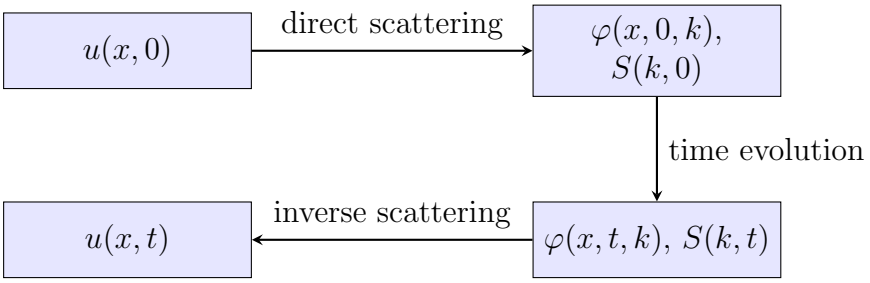

FIGURE 1.2: Initial data $u(x,0)$ is given at $t = 0$. The initial data is mapped to eigenfunctions and scattering data $S(k,0)$ via (1.2). The evolution of the eigenfunctions and scattering data is determined from (1.3). Then $u(x,t)$ can be recovered from inverse scattering.

The IST method is usually applied on the infinite line for the initial data that decay to zero sufficiently fast at infinity. In this case, the time evolution of the KdV equation (1.1) from arbitrary initial data leads to a generation of finitely many interacting solitons and the dispersive waves [16]. Solitons correspond to isolated eigenvalues of the discrete spectrum of the stationary Schrödinger equation (1.2) and the dispersive waves correspond to the continuous spectrum.

In this thesis, however, we do not explore the IST method but instead, work with the Darboux transformation method, which is based on eigenvalues and eigenfunctions of (1.2)-(1.3). The Darboux Transformation is used as a tool for obtaining exact solutions for

interactions of solitons and dispersive wave background. A brief overview of the method is given in the next section.

1.3 The Darboux Transformation for the KdV equation

The Darboux transformation is used as a practical tool for obtaining exact solution of many partial differential equations. This algebraic method dates back to 1882 when G. Darboux [15], first used it in the context of the one-dimensional Schrödinger equation. Even thought the Darboux transformation presents a simpler algebraic alternative to more complicated methods of obtaining explicit solutions, such as the IST method or the Bäcklund transform, the application of Darboux transformation in the context of soliton theory is still sparse. Thus, in this thesis we present, using the Darboux transformation, two different solutions for the KdV equation (1.1), which describe non-trivial soliton - dispersive wave interaction solutions.

The Darboux transformation $u \mapsto \hat{u}$ for the KdV equation (1.1) can be defined as follows [35]. Let u be a bounded solution of the KdV equation (1.1), v_0 be a smooth solution of the linear equations (1.2) and (1.3) with a spectral parameter $\lambda_0 \in \mathbb{R}$, and v be an arbitrary solution of linear equations (1.2) and (1.3) with arbitrary λ. Then

$$\hat{u} := u + 2\frac{\partial^2}{\partial x^2}\log(v_0) \tag{1.5}$$

is a new solution of the KdV equation (1.1) and

$$\hat{v} := \frac{\partial v}{\partial x} - v\frac{\partial}{\partial x}\log(v_0) \tag{1.6}$$

is a solution of the linear equations (1.2) and (1.3) corresponding to $u = \hat{u}$ for the same value of λ as in v. The new solution $\hat{u}(x,t)$ is non-singular if and only if $v_0(x,t) \neq 0$ everywhere in the (x,t) plane. Validity of the transformation formulas (1.5) and (1.6) can be checked by substituting them directly into equations (1.2) and (1.3).

In this work, we will be relying on the integrability of the KdV equation, which allows us to use the Darboux transformation to superimpose a soliton on a dispersive wave background.

In practice, the most difficult task usually involves solving the linear Lax pair (1.2) and (1.3) with the potential $u(x,t)$. Once the eigenfunctions are known, the Darboux Transformation is a routine algebraic procedure. Luckily, motivated by many physical applications, the literature on the stationary Schrödinger equation (1.2) is broad-ranging. For instance, the spectral problem in Chapter 3 involves a well-known Lamé equation, for which the eigenfunctions have already been found more than a centure ago.

Let us now illustrate how the Darboux transformation works by adding a soliton to the zero background. This will serve as a building block and a point of reference of a more complicated interaction solutions discussed in the following chapters.

1.4 One-soliton on the zero background

Suppose the initial condition $u(x,0)$ tends to zero sufficiently rapidly as $x \to \pm\infty$. In this case, the Schrödinger operator has a finite number of bound states and an absolutely continuous spectrum for positive energies.

To solve the direct scattering problem we will follow the scheme outlined in Figure 1.2.

The linear equation (1.3) can be rewritten in the form

$$\frac{\partial v}{\partial t} = (4\lambda - 2u)\frac{\partial v}{\partial x} + (u_x + \gamma)v, \tag{1.7}$$

where we have used $v_{xxx} = -(u+\lambda)v_x - u_x v$ from the spectral equation (1.3) and have added the parameter γ by the transformation $v \mapsto ve^{-\gamma t}$.

Existence of the spatially bounded non-zero solutions $v = v(x,t)$ depends on the values of the spectral parameter λ and should be performed separately in two regions:

$$(1)\ \lambda \in (-\infty, 0), \quad (2)\ \lambda \in (0, \infty).$$

1. **Continuous spectrum $\lambda \in (0,\infty)$: scattering solutions**

   We parameterize positive λ by $\lambda = k^2$, $k \in \mathbb{R}$. The eigenfunctions satisfy the following asymptotic boundary conditions

$$\begin{aligned} &\phi(x;k) \to e^{-ikx}, \quad \bar{\phi}(x;k) \to e^{ikx} \quad x \to -\infty \\ &\psi(x;k) \to e^{ikx}, \quad \bar{\psi}(x;k) \to e^{-ikx}, \quad x \to \infty \end{aligned} \tag{1.8}$$

Each pair $(\phi, \bar{\phi})$ and $(\psi, \bar{\psi})$ contains two linearly independent solutions. Since one pair depends on the other pair, we can introduce the following scattering relation

$$\phi(x;k) = a(k)\bar{\psi}(x;k) + b(k)\psi(x;k) \tag{1.9}$$

where coefficients $a(k)$ and $b(k)$ are referred to as the scattering data.

The time dependence of the scattering data is computed from (1.7). Substituting the asymptotics $\phi(x,t;k) \to e^{-ikx}$, and $u(x,t) \to 0$, as $x \to -\infty$ into (1.7), we obtain the definition of γ

$$\gamma e^{-ikx} - 4ik^3 e^{-ikx} = 0 \implies \gamma = 4ik^3. \tag{1.10}$$

Substituting the asymptotics $\phi(x,t;k) \to a(k;t)e^{-ikx} + b(k;t)e^{ikx}$, and $u(x,t) \to 0$, as $x \to \infty$ into (1.7), we obtain

$$\frac{da}{dt} = 0, \qquad \frac{db}{dt} = 8ik^3 b$$

from which the exact solution is given by

$$a(k;t) = a(k;0), \qquad b(k;t) = b(k;0)e^{8ik^3 t}. \tag{1.11}$$

A time-dependent solution of the stationary Schrödinger equation (1.2) then satisfies

$$\phi(x,t;k) \to \begin{cases} e^{-ikx}, & x \to -\infty \\ a(k;0)e^{-ikx} + b(k;t)e^{ikx}, & x \to \infty \end{cases} \tag{1.12}$$

Definition 1.1. We say that $[0, \infty)$ is **the continuous spectrum** of the stationary Schrödinger equation (1.2).

2. **Discrete spectrum** $\lambda \in (-\infty, 0)$: **bound states**

We parameterize negative λ by $\lambda = -\mu^2$, $\mu > 0$. In this case, there are no oscillatory solutions but instead we have an exponentially decaying eigenfunction $\phi(x,t;\mu)$ as $x \to -\infty$, with the second linearly independent solution $\bar{\phi}(x,t;\mu)$ unbounded as $x \to -\infty$. The only bounded solution as $x \to -\infty$ satisfies

$$\phi(x,t;\mu) \to \begin{cases} e^{\mu x}, & x \to -\infty \\ a(\mu;t)e^{\mu x} + b(\mu;t)e^{-\mu x}, & x \to \infty \end{cases} \tag{1.13}$$

If $a(\mu;t) \neq 0$, then $\phi(x,t;\mu)$ is unbounded as $x \to +\infty$. However, if $a(\mu_0;t) = 0$ for some $\mu_0 \in (0,\infty)$, then the eigenfunction $\phi(x,t;\mu_0)$ is bounded and exponentially decaying as $|x| \to \infty$. The corresponding eigenfunction satisfies

$$\phi(x,t;\mu_0) \to \begin{cases} e^{\mu_0 x}, & x \to -\infty, \\ b_0(t)e^{-\mu_0 x}, & x \to +\infty, \end{cases}$$

Substituting $\phi(x,t;\mu_0) \to +\infty$ into (1.7) we find the time evolution of $b_0(t)$:

$$b_0(t) = b_0(0)e^{4\mu_0^3 t}.$$

Definition 1.2. We say that $\lambda_0 = -\mu_0^2$ is **an isolated eigenvalue** of the stationary Schrödinger equation (1.2) if $a(\mu_0;t) = 0$ for some $\mu_0 \in (0,\infty)$.

Remark 1.3. The bound state problem can be viewed as the analytic continuation of the scattering problem, defined on the real k-axis, to the upper half of the complex k-plane. Then the discrete points of the spectrum are found as simple poles $k = i\mu_0$ of the coefficient $a(k;t) = a(k;0)$, which is time-independent.

Simplest example of the initial condition that decays sufficiently rapidly is the trivial potential $u = 0$. In this case, linear equations (1.2-1.3) reduce to

$$\frac{\partial^2 v}{\partial x^2} + \lambda v = 0 \tag{1.14}$$

$$\frac{\partial v}{\partial t} = -4\frac{\partial^3 v}{dx^3}. \tag{1.15}$$

The isolated eigenvalue of the stationary Schrödinger equation (1.2) corresponds to a soliton of the KdV equation (1.1). Thus, in order to use the Darboux transformation to superimpose soliton on a zero background, we pick the following solution of the linear equations (1.2) and (1.3) with fixed $\lambda = -\mu_0^2 \in (-\infty, 0)$,

$$v_0(t,x) = e^{\mu_0(x-4\mu_0^2 t - x_0)} + e^{-\mu_0(x-4\mu_0^2 t - x_0)},$$

where x_0 is arbitrary. Substituting $u = 0$ and this v_0 into (1.5) yields the well-known one-soliton solution

$$\hat{u}(t,x) = 2\mu_0^2 \operatorname{sech}^2[\mu_0(x - 4\mu_0^2 t - x_0)], \tag{1.16}$$

where μ_0 determines the amplitude $2\mu_0^2$, the width μ_0^{-1}, and the velocity $4\mu_0^2$ of the soliton and x_0 determines the initial location of the soliton. The transformation formula (1.6)

for the second, linear independent solution

$$v(t,x) = e^{\mu_0(x-4\mu_0^2 t - x_0)} - e^{-\mu_0(x-4\mu_0^2 t - x_0)},$$

of the same linear equations (1.2) and (1.3) with $u = 0$ and $\lambda = \lambda_0$ yields the exponentially decaying solution

$$\hat{v}(t,x) = 2\mu_0 \operatorname{sech}[\mu_0(x - 4\mu_0^2 t - x_0)]$$

of the linear equations (1.2) and (1.3) with $u = \hat{u}$ and $\lambda = \lambda_0$. Hence, $\lambda_0 = -\mu_0^2$ is the isolated eigenvalue of the stationary Schrödinger equation (1.2) corresponding to the one-soliton solution (1.16).

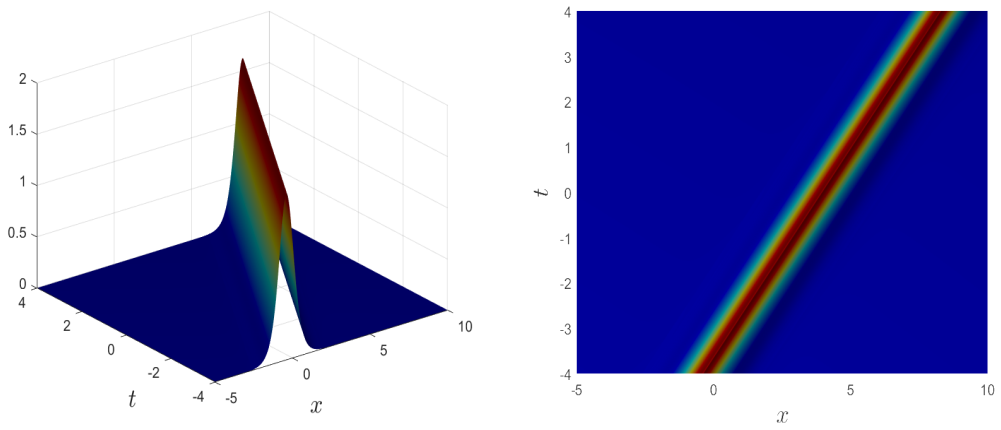

FIGURE 1.3: Soliton travelling on the zero background, given by (1.16), for $\mu = 0.9$ and $x_0 = 0$.

Remark 1.4. Picking solutions of the linear equations (1.2) and (1.3) with fixed $\lambda_0 = k_0^2 \in (0,\infty)$ does not generate bounded solutions of the KdV equation (1.1) by the Darboux transformation. Indeed, a general solution is given by

$$v_0(t,x) = c_1 \cos(k_0 x + 4k_0^3 t) + c_2 \sin(k_0 x + 4k_0^3 t),$$

where (c_1, c_2) are arbitrary constants. Substituting v_0 into (1.5) yields a new solution of the KdV equation (1.1),

$$\hat{u}(t,x) = -\frac{2k_0^2(c_1^2 + c_2^2)}{[c_1 \cos(k_0 x + 4k_0^3 t) + c_2 \sin(k_0 x + 4k_0^3 t)]^2},$$

which is singular at countably many lines in the (x,t) plane where

$$\tan(k_0 x + 4k_0^3 t) = -\frac{c_1}{c_2}.$$

Chapter 2

Solitons on the Rarefaction Wave Background

Motivated by many applications, such as the tidal bores or the earthquake-generated waves, we consider the initial-value problem for the KdV equation (1.1) with the step-like boundary conditions:

$$\lim_{x\to-\infty} u(x,t) = 0, \quad \lim_{x\to+\infty} u(x,t) = c^2, \tag{2.1}$$

where $c^2 > 0$ is a constant.

Evolution of the step-like data results in the appearance of a rarefaction wave (RW) if t advances to positive times or a dispersive shock wave (DSW) if t advances to negative times. In what follows, we will consider the initial-value problem (2.1) for the RW in positive time $t > 0$ since the analysis for negative time $t < 0$ is similar [36].

Compared to initial data that decay to zero sufficiently fast at infinity, for the step boundary conditions (2.1), the dynamics of the KdV equation (1.1) are more interesting. In addition to the RW generated by the step boundary conditions for $t > 0$, a finite number of solitary waves can appear from bumps in the initial data. Depending on the amplitude of these bumps, they either evolve into large-amplitude solitary waves propagating over the RW background with a constant speed or into small-amplitude solitary waves trapped by the RW [36].

Here we analyze the two scenarios of transmitted or trapped solitary wave.

2.1 Main results

The spectrum of the stationary Schrödinger equation (1.2) for the step-like boundary conditions (2.1) was analyzed in [1], where it was shown that the transmitted soliton corresponds to an isolated real eigenvalue. In regards to the trapped soliton, it was related to the so-called "pseuso-embedded" eigenvalue located near a specific point inside the continuous spectrum which does not correspond to a true embedded eigenvalue with exponentially decaying eigenfunctions. Details of where these "pseudo-embedded" eigenvalues are located were not given.

In this chapter we consider the case when a solitary wave is added on the step-like initial data for the KdV equation. The step-like initial data evolves into a rarefaction wave (RW) whereas the solitary wave either propagates over the RW or completely disappears inside the RW. The outcome depends on whether there exists an isolated eigenvalue of the stationary Schrödinger equation outside the continuous spectrum. If it exists, we can construct the transmitted soliton by using the Darboux transformation.

The following theorem presents one of the main results of this chapter. It states that a transmitted soliton can be generated via Darboux transformation.

Theorem 2.1. *Let u be a bounded solution of the KdV equation (1.1) with the boundary conditions (2.1) such that the spectrum of the Schrödinger equation (1.2) is purely continuous in $[-c^2, \infty)$. For every $\lambda_0 < -c^2$, there exists a choice of a smooth function v_0 such that the Darboux transformation (1.5) returns a bounded solution $\hat{u}$ of the KdV equation (1.1) for which the spectrum of the Schrödinger equation (1.2) consists of the purely continuous spectrum in $[-c^2, \infty)$ and a simple isolated eigenvalue λ_0.*

The proof of this theorem can be found in Section 2.4.

If the isolated eigenvalue does not exist in the stationary Schrödinger equation, we show that no embedded eigenvalues exist because zeros of the transmission coefficients that correspond to the soliton, transform into complex resonant poles. This result is more technical, and it is formulated in Theorem 2.6 and proved in Section 2.3.

2.2 Direct scattering transform and the time evolution

Following Section 1.4, where we have considered decaying potentials to zero at infinity, here we review spectral data and their time evolution in the solutions of the linear equations (1.2) and (1.3) for the potential $u = u(x,t)$ satisfying the boundary conditions (2.1). We assume that $u(x,t) \to c^2 H(x)$ as $|x| \to \infty$ sufficiently fast so that all formal expressions can be rigorously justified with Levinson's theorem for differential equations whose variable coefficients are integrable perturbations of the constant coefficients. The notation H stands for the Heaviside step function.

In Chapter 1, we introduced the following form of the linear equation (1.3)

$$\frac{\partial v}{\partial t} = (4\lambda - 2u)\frac{\partial v}{\partial x} + (u_x + \gamma)v, \tag{2.2}$$

where $\gamma = 4ik^3$ is the same since $u(x,t) \to 0$ as $x \to -\infty$.

We are looking for the spatially bounded non-zero solutions $v = v(x,t)$. Existence of such solutions depend on the values of the spectral parameter λ and should be performed separately in three regions, as summarized in Figure 2.1 below:

$$(1)\ \ \lambda \in (0,\infty), \qquad (2)\ \ \lambda \in (-c^2, 0), \qquad (3)\ \ \lambda \in (-\infty, -c^2).$$

The border cases $\lambda = 0$ and $\lambda = -c^2$ can also be included in the consideration but will be omitted to keep the presentation concise.

Continuous spectrum $\lambda \in (0,\infty)$:

We parameterize positive λ as $\lambda = k^2$ with $k > 0$ and introduce

$$\varkappa := \sqrt{c^2 + k^2}$$

such that $\varkappa > 0$.

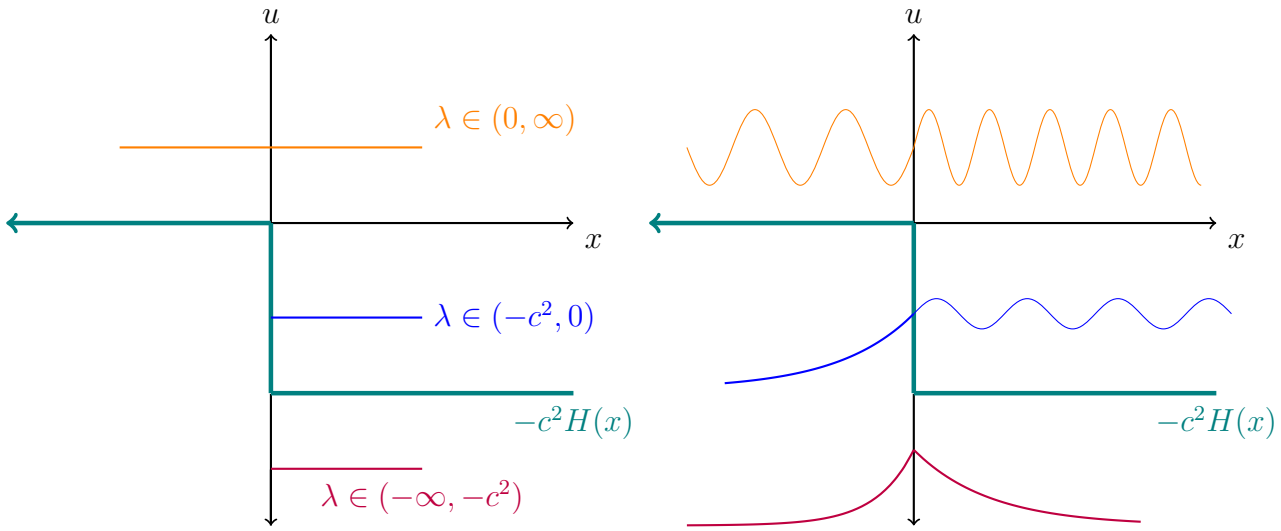

FIGURE 2.1: Left: Admissible values of the spectral parameter λ, corresponding to the potential $u(x,t) \to c^2 H(x)$, $|x| \to \infty$, which satisfies the boundary condition (2.1). Right: Scattering at a step potential of height c^2, shown in green. Eigenfunctions corresponding to λ for each of the three regions are coloured accordingly.

One solution of the stationary Schrödinger equation (1.3) with $u(t,x) \to c^2 H(x)$ as $|x| \to \infty$ is given by $\phi(x,t;k)$ satisfying

$$\phi(x,t;k) \to \begin{cases} e^{-ikx}, & x \to -\infty, \\ a(k;t)e^{-i\varkappa x} + b(k;t)e^{i\varkappa x}, & x \to +\infty. \end{cases} \tag{2.3}$$

The second linearly independent eigenfunction is given by $\phi(x,t;-k)$ with the same $\varkappa$. Both solutions are oscillatory on $\mathbb{R}$ and do not decay to zero at infinity.

Substituting the asymptotics $\phi(x,t;k) \to a(k;t)e^{-i\varkappa x} + b(k;t)e^{i\varkappa x}$ and $u(x,t) \to c^2$ as $x \to +\infty$ into (2.2) and using $\gamma = 4ik^3$ we obtain

$$\begin{aligned} \frac{da}{dt} &= i(4k^3 - 4k^2\varkappa + 2c^2\varkappa)a, \\ \frac{db}{dt} &= i(4k^3 + 4k^2\varkappa - 2c^2\varkappa)b, \end{aligned}$$

from which the exact solution is given by

$$a(k;t) = a(k;0)e^{i(4k^2(k-\varkappa)+2c^2\varkappa)t}, \qquad b(k;t) = b(k;0)e^{i(4k^2(k+\varkappa)-2c^2\varkappa)t}. \tag{2.4}$$

Compared to the case of decaying initial conditions, i.e., $c = 0$, it is no longer true that $a(k;t)$ is constant in t.

Continuous spectrum $\lambda \in (-c^2, 0)$:

We parameterize negative λ by $\lambda = -\mu^2$ with $\mu \in (0, c)$ and introduce

$$\varkappa := \sqrt{c^2 - \mu^2}$$

such that $\varkappa > 0$. For the sake of notations, we redefine $\phi(x,t;k)$, $a(k;t)$, and $b(k;t)$ for $k = i\mu$ with $\mu > 0$ as $\phi(x,t;\mu)$, $a(\mu;t)$, and $b(\mu;t)$. We do not assume here any analyticity assumptions on the eigenfunctions and scattering data. The only bounded solution as $x \to -\infty$ is obtained from (2.3) with $k = i\mu$ as $\phi(x,t;\mu)$ satisfying

$$\phi(x,t;\mu) \to \begin{cases} e^{\mu x}, & x \to -\infty, \\ a(\mu;t)e^{-i\varkappa x} + b(\mu;t)e^{i\varkappa x}, & x \to +\infty. \end{cases} \tag{2.5}$$

The other solution $\phi(x,t;-\mu)$ is exponentially growing as $x \to -\infty$.

Time evolution of the scatering data is obtained from (2.4) with the same change $k = i\mu$:

$$a(\mu;t) = a(\mu;0)e^{(4\mu^2(\mu+i\varkappa)+2ic^2\varkappa)t}, \qquad b(\mu,t) = b(\mu;0)e^{(4\mu^2(\mu-i\varkappa)-2ic^2\varkappa)t}. \tag{2.6}$$

Note that $\phi(x,t;\mu)$ decays to zero as $x \to -\infty$ but is oscillatory as $x \to +\infty$.

Discrete spectrum $\lambda \in (-\infty, -c^2)$:

We use the same parameterization $\lambda = -\mu^2$ with $\mu > c$ and introduce

$$\nu := \sqrt{\mu^2 - c^2}$$

such that $\nu > 0$. The only bounded solution as $x \to -\infty$ is obtained from (2.5) with $\varkappa = i\nu$ so that $\phi(x,t;\mu)$ satisfies

$$\phi(x,t;\mu) \to \begin{cases} e^{\mu x} & x \to -\infty, \\ a(\mu;t)e^{\nu x} + b(\mu;t)e^{-\nu x} & x \to +\infty. \end{cases} \tag{2.7}$$

The second linearly independent solution $\phi(x,t;-\mu)$ is exponentially growing as $x \to -\infty$. If $a(\mu;t) \neq 0$, then $\phi(x,t;\mu)$ is unbounded as $x \to +\infty$. However, if $a(\mu_0;t) = 0$ for some $\mu_0 \in (c, \infty)$, then the eigenfunction $\phi(x,t;\mu_0)$ is bounded and exponentially decaying as

$|x|\to\infty$. The corresponding eigenfunction satisfies

$$\phi(x,t;\mu_0) \to \begin{cases} e^{\mu_0 x}, & x \to -\infty, \\ b_0(t)e^{-\nu_0 x}, & x \to +\infty, \end{cases}$$

where $\nu_0 := \sqrt{\mu_0^2 - c^2}$ and $b_0(t)$ satisfies the time evolution that follows from (2.6):

$$b_0(t) = b_0(0)e^{(4\mu_0^2(\mu_0+\nu_0)+2c^2\nu_0)t}.$$

Note that $\phi(x,t;\mu_0)$ is exponentially decaying as $x \to \pm\infty$ with two different decay rates: μ_0 at $-\infty$ and ν_0 at $+\infty$.

2.3 Examples of the step-like initial conditions

Here we solve the scattering problem for two simplest initial conditions satisfying the boundary conditions (2.1). Since the time evolution of the scattering data is not considered, we drop t from the list of arguments.

Case of the step function $u_0(x) = c^2 H(x)$.

For $\lambda \in (0,\infty)$, the eigenfunction is given by (2.3), where the superposition of exponential functions hold for every $x < 0$ and $x > 0$, not just in the limits $x \to -\infty$ and $x \to +\infty$. Since ϕ and ϕ' must be continuous at $x = 0$, we derive the system of linear equations for $a(k)$ and $b(k)$:

$$\begin{cases} 1 = a(k) + b(k), \\ -ik = i\varkappa b(k) - i\varkappa a(k). \end{cases}$$

The linear system admits a unique solution given by

$$a(k) = \frac{\varkappa + k}{2\varkappa}, \qquad b(k) = \frac{\varkappa - k}{2\varkappa}. \tag{2.8}$$

Similarly, for $\lambda \in (-c^2, 0)$, the scattering data $a(\mu)$ and $b(\mu)$ are obtained from (2.8) by substituting $k = i\mu$ with $\mu > 0$:

$$a(\mu) = \frac{\varkappa + i\mu}{2\varkappa}, \qquad b(\mu) = \frac{\varkappa - i\mu}{2\varkappa}. \tag{2.9}$$

No zeros of $a(\mu)$ exists for $\lambda \in (-\infty, -c^2)$ since $a(\mu)$ is given by the same expression (2.9) but with $\varkappa = i\nu$ and $\nu + \mu = \sqrt{\mu^2 - c^2} + \mu > 0$. The spectrum of the stationary Schrödinger equation (1.2) is purely continuous.

Remark 2.2. The step function can be replaced by the smooth function

$$u_0(x) = \frac{1}{2}c^2 \left[1 + \tanh(\varepsilon x)\right], \quad \varepsilon > 0. \tag{2.10}$$

Exact solutions for the scattering data $a(k)$ and $b(k)$ associated with u_0 in (2.10) are available in the literature [38]. The spectrum of the stationary Schrödinger equation (1.2) is also purely continuous. We use (2.10) instead of $c^2 H(x)$ in numerical experiments to reduce the numerical noise generated by the singular step function.

Case of a soliton on the step function.

We consider a linear superposition of a soliton and the step function:

$$u_0(x) = 2\mu_0^2 \operatorname{sech}^2(\mu_0(x - x_0)) + c^2 H(x), \tag{2.11}$$

where $\mu_0 > 0$ is the soliton parameter and $x_0 < 0$ is chosen to ensure that the soliton is located to the left of the step function. The direct scattering problem for the initial condition (2.11) was solved in [1] and here we extend the solution with more details.

The spectral problem (1.2) with $u = u_0$ can be solved exactly [38]. For $x < 0$, the exact solution for $\phi(x;k)$ satisfying $\phi(x;k) \to e^{-ikx}$ as $x \to -\infty$ is given by

$$\phi(x;k) = e^{-ikx}\left[1 - \frac{i\mu_0}{k + i\mu_0} e^{\mu_0(x-x_0)} \operatorname{sech}(\mu_0(x - x_0))\right], \quad x < 0.$$

Similarly for $x > 0$, the exact solution for $\psi(x;k)$ satisfying $\psi(x;k) \to e^{i\varkappa x}$ as $x \to +\infty$ is given by

$$\psi(x;k) = e^{i\varkappa x}\left[1 - \frac{i\mu_0}{\varkappa + i\mu_0} e^{-\mu_0(x-x_0)} \operatorname{sech}(\mu_0(x - x_0))\right], \quad x > 0.$$

The scattering data $a(k)$ and $b(k)$ in the representation (2.3) can be found from the scattering relation

$$\phi(x;k) = a(k)\overline{\psi}(x;k) + b(k)\psi(x;k), \quad x \in \mathbb{R},$$

where $\overline{\psi}(x;k)$ is obtained from $\psi(x;k)$ by reflection $\varkappa \mapsto -\varkappa$. Since the Wronskian $W(\psi_1, \psi_2)$ of any two solutions ψ_1 and ψ_2 of the stationary Schrödinger equation (1.2) is

independent of x, the scattering coefficient $a(k)$ can be obtained from the formula:

$$a(k) = \frac{W(\phi(x;k), \psi(x;k))}{W(\bar{\psi}(x;k), \psi(x;k))}, \quad x \in \mathbb{R}. \tag{2.12}$$

Since we are free to choose $x = 0$ in (2.12), we compute

$$\begin{aligned} W(\bar{\psi}, \psi)|_{x=0} =& 2i\varkappa \left(1 + \frac{i\mu_0 e^{\mu_0 x_0} \operatorname{sech}(\mu_0 x_0)}{\varkappa - i\mu_0}\right)\left(1 - \frac{i\mu_0 e^{\mu_0 x_0} \operatorname{sech}(\mu_0 x_0)}{\varkappa + i\mu_0}\right) \\ &+ \frac{i\mu_0^2 \operatorname{sech}^2(\mu_0 x_0)}{\varkappa - i\mu_0}\left(1 - \frac{i\mu_0 e^{\mu_0 x_0} \operatorname{sech}(\mu_0 x_0)}{\varkappa + i\mu_0}\right) \\ &+ \frac{i\mu_0^2 \operatorname{sech}^2(\mu_0 x_0)}{\varkappa + i\mu_0}\left(1 + \frac{i\mu_0 e^{\mu_0 x_0} \operatorname{sech}(\mu_0 x_0)}{\varkappa - i\mu_0}\right) \\ &= 2i\varkappa \end{aligned}$$

and

$$\begin{aligned} W(\phi, \psi)|_{x=0} =& i(\varkappa + k)\left(1 - \frac{i\mu_0 e^{\mu_0 x_0} \operatorname{sech}(\mu_0 x_0)}{\varkappa + i\mu_0}\right)\left(1 - \frac{i\mu_0 e^{\mu_0 x_0} \operatorname{sech}(\mu_0 x_0)}{\varkappa + i\mu_0}\right) \\ &+ \frac{i\mu_0^2 \operatorname{sech}^2(\mu_0 x_0)}{\varkappa + i\mu_0}\left(1 - \frac{i\mu_0 e^{-\mu_0 x_0} \operatorname{sech}(\mu_0 x_0)}{k + i\mu_o}\right) \\ &+ \frac{i\mu_0^2 \operatorname{sech}^2(\mu_0 x_0)}{k + i\mu_0}\left(1 - \frac{i\mu_0 e^{\mu_0 x_0} \operatorname{sech}(\mu_0 x_0)}{\varkappa + i\mu_0}\right) \\ &= \frac{i(\varkappa + k)(\varkappa k + \mu_0^2 + i\mu_0(\varkappa - k)\tanh(\mu_0 x_0))}{(\varkappa + i\mu_0)(k + i\mu_0)}, \end{aligned}$$

which yields

$$a(k) = \frac{(\varkappa + k)\,(\varkappa k + \mu_0^2 + i\mu_0(\varkappa - k)\tanh(\mu_0 x_0))}{2\varkappa(\varkappa + i\mu_0)(k + i\mu_0)}. \tag{2.13}$$

This expression coincides with (A6) in [1] up to notations.

Although the previous expressions were obtained for $\lambda = k^2 > 0$ with $k \in \mathbb{R}$, the scattering coefficient $a(k)$ can be continued analytically for $k \in \mathbb{C}$ with $\operatorname{Im}(k) \geq 0$. However, $k = ic$ is a branch point for the square root function for $\varkappa := \sqrt{c^2 + k^2}$. The branch cuts can be defined at our disposal on the imaginary axis, $\operatorname{Re}(k) = 0$, for which $\operatorname{Im}(k)$ takes values on

$$\text{either } \ [-c, c] \ \text{ or } \ (-\infty, -c] \cup [c, \infty).$$

Notations. The square root function $\sqrt{z}$ for $z \in \mathbb{C}$ is defined according to the principal branch such that $\operatorname{Arg}(\sqrt{z}) \in [0, \pi)$ for every $z \in \mathbb{C}$ with $\operatorname{Arg}(z) \in [0, 2\pi)$.

We are looking for zeros of $a(k)$ for $\text{Im}(k) > 0$ for which $\phi(x;k) \to 0$ as $x \to -\infty$.

Definition 2.3. If $a(k_0) = 0$ with $\text{Im}(k_0) \in (c, \infty)$ corresponds to $\varkappa_0 := \sqrt{c^2 + k_0^2}$ satisfying $\text{Im}(\varkappa_0) > 0$, then $\phi(x;k_0) = b_0\psi(x;k_0) \to 0$ as $x \to +\infty$. This yields **the eigenvalue** $\lambda_0 := k_0^2$ of the spectral problem (1.2), for which the branch cut can be chosen for $\text{Re}(k) = 0$ and $\text{Im}(k) \in [-c, c]$. In this case, the spectral theory of the Schrödinger equation (1.2) implies that $\text{Re}(k_0) = 0$ and $\text{Re}(\varkappa_0) = 0$.

Definition 2.4. If $a(k_0) = 0$ with $\text{Im}(k_0) \in (0, c)$ corresponds to $\varkappa_0 := \sqrt{c^2 + k_0^2}$ satisfying $\text{Re}(\varkappa_0) > 0$ and $\text{Im}(\varkappa_0) < 0$, then $\phi(x;k_0) = b_0\psi(x;k_0) \to \infty$ as $x \to +\infty$. In this case, we say that $\lambda_0 := k_0^2$ is **the resonant pole** of the spectral problem (1.2). The branch cut can be chosen for $\text{Re}(k) = 0$ and $\text{Im}(k) \in (-\infty, -c] \cup [c, \infty)$. Moreover, $\text{Re}(k_0) \neq 0$ if $\text{Re}(\varkappa_0) > 0$, and $\text{Im}(\varkappa_0) < 0$.

Remark 2.5. The coefficient b_0 in $\phi(x;k_0) = b_0\psi(x;k_0)$ for which $a(k_0) = 0$ can not be associated with $b(k_0)$ because the scattering coefficient $b(k)$ is not analytically continued off the real axis unlike the scattering coefficient $a(k)$.

We are now in position to analyze zeros of $a(k)$ given by (2.13). The following proposition presents the main outcome of this analysis.

Theorem 2.6. *For sufficiently large negative x_0, an isolated eigenvalue $\lambda_0 \in (-\infty, -c^2)$ persists near $-\mu_0^2$ if $\mu_0 \in (c, \infty)$, whereas the embedded eigenvalue $\lambda_0 \in (-c^2, 0)$ moves to a resonant pole with $\text{Re}(k_0) < 0$ if $\mu_0 \in (0, c)$.*

Proof. Since $\varkappa + k \neq 0$, it follows from (2.13) that $a(k) = 0$ if and only if k is the root of the following transcendental equation

$$\varkappa k + \mu_0^2 + i\mu_0(\varkappa - k)\tanh(\mu_0 x_0) = 0. \tag{2.14}$$

The algebraic equation (2.14) is factorized in the limit $x_0 \to -\infty$ as $(\varkappa + i\mu_0)(k - i\mu_0) = 0$. Hence, there exists a simple root $k = i\mu_0$ in the limit $x_0 \to -\infty$. If $\mu_0 \in (c, \infty)$, this root corresponds to the eigenvalue $\lambda = -\mu_0^2 \in (-\infty, -c^2)$, however, if $\mu_0 \in (0, c)$, the root corresponds to the embedded eigenvalue $\lambda = -\mu_0^2 \in (-c^2, 0)$ in the continuous spectrum. We consider the two cases separately.

Isolated eigenvalue if $\mu_0 \in (c, \infty)$.

Since $\tanh(\mu_0 x_0) = -1 + 2e^{2\mu_0 x_0} + \mathcal{O}(e^{4\mu_0 x_0})$ as $x_0 \to -\infty$, the simple root of equation (2.14) can be extended asymptotically as follows:

$$k = i\mu_0 \left[1 - 2\left(\frac{\varkappa_0 - i\mu_0}{\varkappa_0 + i\mu_0}\right) e^{2\mu_0 x_0} + \mathcal{O}(e^{4\mu_0 x_0})\right], \tag{2.15}$$

where $\varkappa_0 := \sqrt{c^2 - \mu_0^2} = i\sqrt{\mu_0^2 - c^2}$ if $\mu_0 > c$. Therefore, $k \in i\mathbb{R}$ in the first two terms. Similarly, we have expansion for $\varkappa^2 = c^2 + k^2$ given by

$$\varkappa = \varkappa_0 \left[1 - \frac{2\mu_0^2}{\mu_0^2 - c^2} e^{2\mu_0 x_0} \left(\frac{\varkappa_0 - i\mu_0}{\varkappa_0 + i\mu_0}\right) + \mathcal{O}(e^{4\mu_0 x_0})\right], \tag{2.16}$$

so that $\varkappa \in i\mathbb{R}$ in the first two terms. In order to show that $k, \varkappa \in i\mathbb{R}$ persists beyond the first two terms, we substitute $k = i\mu$ and $\varkappa = i\nu$ with $\nu = \sqrt{\mu^2 - c^2}$ into (2.14) and obtain the real-valued equation $F(\mu, \alpha) = 0$, where

$$F(\mu, \alpha) := \mu\sqrt{\mu^2 - c^2} - \mu_0^2 + \mu_0(\sqrt{\mu^2 - c^2} - \mu)\alpha, \quad \alpha := \tanh(\mu_0 x_0). \tag{2.17}$$

The function $F(\mu, \alpha) : \mathbb{R}^2 \mapsto \mathbb{R}$ is a C^1 function near $(\mu, \alpha) = (\mu_0, -1)$ satisfying $F(\mu_0, -1) = 0$ and

$$\partial_\mu F(\mu_0, -1) = \sqrt{\mu_0^2 - c^2} + \mu_0 \neq 0.$$

By the implicit function theorem, there exists a simple real root $\mu \in (c, \infty)$ of $F(\mu, \alpha) = 0$ for every $x_0 \ll -1$ ($\alpha \approx -1$) such that $\mu \to \mu_0$ as $x_0 \to -\infty$ ($\alpha \to -1$). Since $k = i\mu \in i\mathbb{R}$ and $\varkappa = i\sqrt{\mu^2 - c^2} \in i\mathbb{R}$, the simple real root $\mu \in (c, \infty)$ determines an isolated eigenvalue $\lambda = -\mu^2 \in (-\infty, -c^2)$ of the spectral problem (1.2).

Resonant pole if $\mu_0 \in (0, c)$.

In this case we have $\varkappa_0 = \sqrt{c^2 - \mu_0^2} \in \mathbb{R}$ so that k and $\varkappa$ in (2.15) and (2.16) are no longer purely imaginary. Since

$$\frac{\varkappa_0 - i\mu_0}{\varkappa_0 + i\mu_0} = \frac{(\varkappa_0 - i\mu_0)^2}{\varkappa_0^2 + \mu_0^2} = \frac{1}{c^2}(c^2 - 2\mu_0^2 - 2i\mu_0\varkappa_0),$$

we obtain from (2.15) and (2.16) that

$$\text{Re}(k) = -\frac{4\mu_0^2}{c^2}\sqrt{c^2 - \mu_0^2} e^{2\mu_0 x_0} + \mathcal{O}(e^{4\mu_0 x_0})$$

and

$$\text{Im}(\varkappa) = -\frac{4\mu_0^3}{c^2} e^{2\mu_0 x_0} + \mathcal{O}(e^{4\mu_0 x_0}).$$

Hence, $\mathrm{Re}(k) < 0$ and $\mathrm{Im}(\varkappa) < 0$ for the root of the complex-valued equation $F(\mu, \alpha) = 0$, which still exists for $x_0 \ll -1$ by the same application of the implicit function theorem. Therefore, the eigenfunction $\phi(x; k)$ for this root k satisfies $\phi(x; k) \to 0$ as $x \to -\infty$ because $\mathrm{Im}(k) > 0$ but $\phi(x; k) = b_0\psi(x; k) \to \infty$ as $x \to +\infty$ because $\mathrm{Im}(\varkappa) < 0$. Thus, this root corresponds to the resonant pole $\lambda = k^2$ with $\mathrm{Re}(\lambda) \in (-c^2, 0)$ and $\mathrm{Im}(\lambda) < 0$, for which the eigenfunction $\phi(x; k)$ decays exponentially at $-\infty$ and diverges exponentially at $+\infty$. □

Remark 2.7. There exists a symmetric resonant pole $-\bar{k}$ relative to $i\mathbb{R}$ if $\varkappa = -\sqrt{c^2 + k^2}$ is defined according to the second branch of the square root function. The corresponding eigenfunction is associated with the same function $\phi(x; k)$ that decays exponentially at $-\infty$ because $\mathrm{Im}(k) > 0$ but grows exponentially at $+\infty$ as $\phi(x; k) = b_0\psi(x; k)$ because $\mathrm{Re}(k) > 0$, $\mathrm{Re}(\varkappa) < 0$, and $\mathrm{Im}(\varkappa) < 0$.

Remark 2.8. It was missed in [1] that the "pseudo-embedded" eigenvalue near $\lambda = -\mu_0^2 \in (-c^2, 0)$ splits into a pair of resonant poles. There exists no embedded eigenvalues in the spectral problem (1.2) if $\mu_0 \in (0, c)$.

2.4 Proof of Theorem 2.1

Let λ_0 be fixed, so that $\lambda_0 = -\mu_0^2 \in (-\infty, -c^2)$, with $\mu_0 \in (c, \infty)$. Then for $a(\mu_0; t) \neq 0$ there exists a solution $\phi(t, x; \mu_0)$ of the linear system (1.2) and (1.3) satisfying the boundary behavior (2.7) so that $\phi(x, t; \mu_0) \to 0$ as $x \to -\infty$ and $\phi(x, t; \mu_0) \to \infty$ as $x \to +\infty$. By the Sturm's theorem, $\phi(x, t; \mu_0) > 0$ for every (x, t) since λ_0 is below the spectrum of the Schrödinger equation (1.2) for every $t \in \mathbb{R}$. Similarly, there exists a strictly positive solution $\psi(x, t; \mu_0)$ satisfying $\psi(x, t; \mu_0) \to 0$ as $x \to +\infty$ and $\psi(x, t; \mu_0) \to \infty$ as $x \to -\infty$. If c_1 and c_2 are positive constants,

$$v_0(x, t) = c_1\phi(x, t; \mu_0) + c_2\psi(x, t; \mu_0)$$

is positive everywhere so that the Darboux transformation (1.5) yields a bounded solution $\hat{u}$. Let d_1 and d_2 be arbitrary satisfying $c_1d_2 - c_2d_1 \neq 0$ and define

$$v(x, t) = d_1\phi(x, t; \mu_0) + d_2\psi(x, t; \mu_0).$$

Due to the decay and divergence conditions on $\phi(t,x;\mu_0)$ and $\psi(x,t;\mu_0)$, the transformation (1.6) yields an exponentially decaying solution

$$\hat{v} = (c_1 d_2 - c_2 d_1)\frac{(\phi(x,t;\mu_0)\partial_x\psi(x,t;\mu_0) - \psi(x,t;\mu_0)\partial_x\phi(x,t;\mu_0))}{c_1\phi(x,t;\mu_0) + c_2\psi(x,t;\mu_0)}$$

of the Schrödinger equation (1.2) for $\lambda = \lambda_0$. Hence $\lambda_0 \in (-\infty, -c^2)$ is an isolated eigenvalue, which is also simple by the Sturm theorem. For every other value of λ, the transformation (1.6) returns bounded solutions if $\lambda \in [-c^2, \infty)$ and unbounded solutions if $\lambda \in (-\infty, -c^2)\backslash\{\lambda_0\}$ so that the spectrum of the Schrödinger equation (1.2) associated with the new solution $\hat{u}$ consists of the purely continuous spectrum in $[-c^2, \infty)$ and a simple isolated eigenvalue λ_0.

2.5 Example of a transmitted soliton

Here we illustrate the Darboux transformation for the transmitted soliton by considering initial data $u_0(x) = c^2 H(x)$ at $t = 0$, and drop t from the list of arguments. We use the following solution of the stationary Schrödinger equation (1.2) with $u = u_0$ and $\lambda = -\mu_0^2 \in (-\infty, -c^2)$ with $\mu_0 \in (c, \infty)$,

$$v_0(x) = \begin{cases} e^{\mu_0(x-x_0)} + e^{-\mu_0(x-x_0)}, & x < 0, \\ c_1 e^{\nu_0 x} + c_2 e^{-\nu_0 x}, & x > 0, \end{cases}$$

where $\nu_0 := \sqrt{\mu_0^2 - c^2} > 0$, x_0 is arbitrary, and (c_1, c_2) are found from the continuity of v_0 and v_0' across $x = 0$. Setting up and solving the linear system for (c_1, c_2) similar to (2.8), we obtain the unique solution

$$\begin{cases} c_1 = \frac{\nu_0+\mu_0}{2\nu_0} e^{-\mu_0 x_0} + \frac{\nu_0-\mu_0}{2\nu_0} e^{\mu_0 x_0}, \\ c_2 = \frac{\nu_0-\mu_0}{2\nu_0} e^{-\mu_0 x_0} + \frac{\nu_0+\mu_0}{2\nu_0} e^{\mu_0 x_0}, \end{cases}$$

Substituting v_0 into (1.5) yields the initial condition, where one soliton is superposed to the step function:

$$\hat{u}_0(x) = 2\mu_0^2 \operatorname{sech}^2[\mu_0(x - x_0)], \quad x < 0 \tag{2.18}$$

and

$$\hat{u}_0(x) = c^2 + 4\nu_0^2 \frac{\nu_0^2 + \mu_0^2 + (\nu_0^2 - \mu_0^2)\cosh(2\mu_0 x_0)}{\left[(\nu_0 + \mu_0)\cosh(\nu_0 x - \mu_0 x_0) + (\nu_0 - \mu_0)\cosh(\nu_0 x + \mu_0 x_0)\right]^2}, \tag{2.19}$$

for $x > 0$. The denominator of (2.19) is strictly positive for every $x_0 \in (-\infty, x_*)$, where x_* is the unique positive root of the transcendental equation

$$\cosh(2\mu_0 x_0) = \frac{\mu_0 + \nu_0}{\mu_0 - \nu_0} > 1.$$

If $x_0 = x_*$, the expression (2.19) is singular at $x = \mu_0 x_0/\nu_0$ and if $x_0 \in (x_*, \infty)$, there exist two singularities of (2.19) on $(0, \infty)$ before and after the value $x = \mu_0 x_0/\nu_0$. The transmitted soliton corresponds to the value of x_0 inside $(-\infty, x_*)$.

Remark 2.9. The one-soliton $\hat{u}_0$ decays differently as $x \to -\infty$ and as $x \to +\infty$, according to (2.18) and (2.19). The decay rate μ_0 at $-\infty$ corresponds to the zero boundary condition, whereas the decay rate $\nu_0 = \sqrt{\mu_0^2 - c^2}$ at $+\infty$ corresponds to the nonzero boundary condition c^2. Due to this discrepancy, the one-soliton obtained by the Darboux transformation is different from the initial condition (2.11) which has the same decay rate μ_0 at $\pm\infty$. In addition, the former is related to the isolated eigenvalue $\lambda_0 = -\mu_0^2$, whereas the latter is related to the isolated eigenvalue $\lambda = k_0^2$ with $k_0 = i\mu_0 + \mathcal{O}(e^{2\mu_0 x_0})$ given by (2.15).

Remark 2.10. The one-soliton on the initial step for $\lambda = -\mu_0^2 \in (-\infty, -c^2)$ corresponds to the transmitted soliton which overtakes the RW in the time dynamics of the KdV equation (1.1). The corresponding time-dependent solution can be constructed from the Darboux transformation with the RW solution $u = u(x,t)$. Since solutions $u(x,t)$ and $v_0(x,t)$ are not explicit, we do not obtain $\hat{u}(x,t)$ in the explicit form for $t \neq 0$.

Remark 2.11. If $\lambda = -\mu_0^2 \in (-c^2, 0)$ with $\mu_0 \in (0, c)$, solution of the stationary Schrödinger equation (1.2) is a bounded and oscillatory function for $x > 0$. Darboux transformation (1.5) generates unbounded solution $\hat{u}_0(x)$ at a countable set of points for $x > 0$ similarly to Remark 1.4. No trapped soliton can be constructed by the Darboux transformation for $\lambda \in (-c^2, 0)$ because no embedded eigenvalues with spatially decaying eigenfunctions exist.

Remark 2.12. If $\lambda = k_0^2 \in (0, \infty)$, then solutions of the stationary Schrödinger equation (1.2) are bounded and oscillatory both for $x < 0$ and $x > 0$. Darboux transformation (1.5) generates unbounded solution $\hat{u}_0(x)$ at countable sets of points both for $x < 0$ and $x > 0$.

2.6 Numerical approximations

Here we perform the time-dependent computations of the KdV equation (1.1). We utilize here the finite-difference method introduced by N. Zabusky and M. Kruskal in [48] for numerical solution of the KdV equation (1.1).

Let u_n^m be a numerical approximation of $u(x_n, t_m)$ on the equally spaced grid $\{x_n\}$ with the equally space times $\{t_m\}$. The time step is τ and the spatial step size is h. The two-point numerical method in [48] is given by

$$u_n^{m+1} = u_n^{m-1} - \frac{2\tau}{h}(u_{n+1}^m + u_n^m + u_{n-1}^m)(u_{n+1}^m - u_{n-1}^m) - \frac{\tau}{h^3}(u_{n+2}^m - 2u_{n+1}^m + 2u_{n-1}^m - u_{n-2}^m).$$

The first step is performed separately with the Euler method

$$u_n^1 = u_n^0 - \frac{\tau}{h}(u_{n+1}^0 + u_n^0 + u_{n-1}^0)(u_{n+1}^0 - u_{n-1}^0) - \frac{\tau}{2h^3}(u_{n+2}^0 - 2u_{n+1}^0 + 2u_{n-1}^0 - u_{n-2}^0).$$

The finite-difference method is stable if $\tau < \frac{2}{3\sqrt{3}}h^3$ for small h [48]. To avoid oscillations of solutions due to the step background, we use the smooth function (2.10) superposed with the soliton (2.11) so that the initial data is

$$u_0(x) = 2\mu_0^2 \operatorname{sech}^2(\mu_0(x - x_0)) + \frac{1}{2}c^2\left[1 + \tanh(\varepsilon x)\right], \tag{2.20}$$

where $x_0 < 0$ and $\varepsilon = 1$.

Outcomes of numerical computations. Evolution of the KdV equation (1.1) with the initial data (2.20) depends on the amplitude of $2\mu_0^2$ of the solitary wave to the left of the step-like background. Figure 2.2 shows three snapshots of the evolution with $\mu_0 = 1.4 > c = 1$. A travelling solitary wave with a sufficiently large amplitude reaches and overtakes the RW formed from the step-like background. This corresponds to dynamics of the transmitted soliton.

Figure 2.3 shows three snapshots of the evolution with $\mu_0 = 0.95 < c = 1$. A travelling solitary wave with a sufficiently small amplitude becomes trapped inside the RW and does not reach its top. This corresponds to dynamics of the trapped soliton.

The left panel of Figure 2.4 shows the spectrum of the stationary Schrödinger equation (1.2) for the initial condition (2.20) with $\mu = 1.4$. The spectrum consists of the continous spectrum on $[-c^2, \infty)$ and an isolated eigenvalue $\lambda_0 < -c^2$. The isolated eigenvalue is

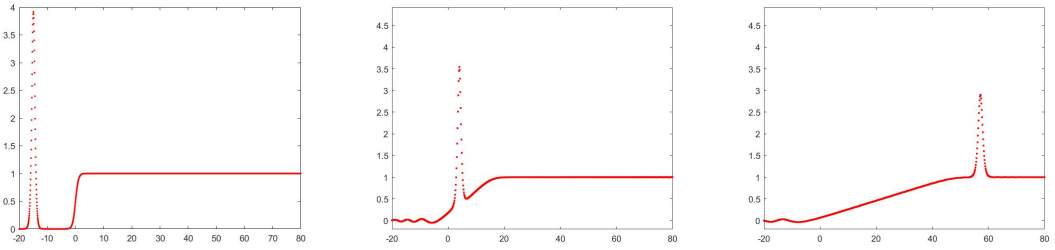

(A) (B) (C)

FIGURE 2.2: The time evolution of a transmitted soliton for $\mu = 1.4$, $c = 1$, $x_0 = -15$, and $\varepsilon = 1$ at $t = 0$ (left), $t = 4$ (middle), and $t = 8$ (right).

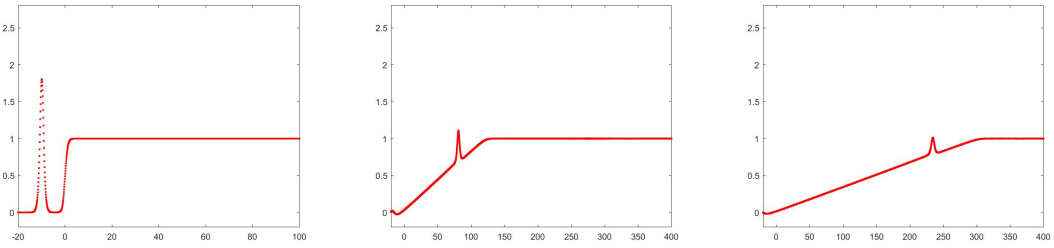

(A) (B) (C)

FIGURE 2.3: The time evolution of a trapped soliton for $\mu = 0.95$, $c = 1$, $x_0 = -10$, and $\varepsilon = 1$ at $t = 0$ (left) $t = 20$ (middle), and $t = 40$ (right).

superimposed with the approximation obtained from the numerically computed root of the function (2.17). The difference between the two approximation is not visible on the scale of the figure, it is of the order of $\mathcal{O}(10^{-3})$. The right panel shows the spectrum for $\mu = 0.95$, for which no isolated or embedded eigenvalues exist.

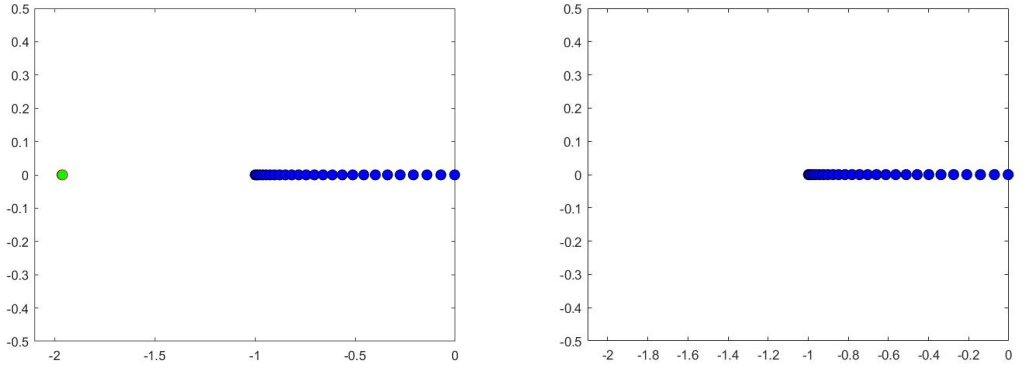

(A) (B)

FIGURE 2.4: Spectrum of the stationary Schrödinger equation (1.2) for $\mu = 1.4$ (left) and $\mu = 0.95$ (right) with the potential u_0 given by (2.20).

Data analysis. We will elaborate the numerical criterion to show that the trapped soliton disappears in the long-time dynamics of the RW. In other words, the solitary wave

does not appear to be a proper soliton on the RW background but is instead completely absorbed by the RW.

Let a^2 be the constant background (which may change in time). The solitary wave on the constant background is obtained from the soliton on the zero background (1.16) with the Galilean transformation:

$$u(x,t) = a^2 + 2\nu_0^2 \mathrm{sech}^2[\nu_0(x - 4\nu_0^2 t - 6a^2 t - x_0)], \tag{2.21}$$

where $\nu_0 > 0$ is the soliton parameter. As follows from the construction of one-soliton on the constant background with the Darboux transformation, see expressions (2.18) and (2.19), ν_0 is related to the fixed value μ_0 (determined for $a = 0$) by $\nu_0 = \sqrt{\mu_0^2 - a^2}$ as long as $a < \mu_0$. Hence the amplitude of the soliton (2.21) on the constant background a^2 is

$$A = a^2 + 2\nu_0^2 = 2\mu_0^2 - a^2.$$

When the solitary wave advances to the RW from the left and is strongly localized on the long scale of the RW like on Figures 2.2 and 2.3, the background a^2 is determined by the value of the RW at the location of the solitary wave.

The RW background can be approximated by the solution of the inviscid Burgers' equation $u_t + 6uu_x = 0$ starting with the piecewise linear profile

$$u_0(x) = \begin{cases} 0, & x < -\varepsilon, \\ (2\varepsilon)^{-1}(x + \varepsilon), & -\varepsilon \le x \le \varepsilon, \\ 1, & x > \varepsilon \end{cases}$$

Solving the inviscid Burgers' equation with $u(0,x) = u_0(x)$ yields

$$u(x,t) = \begin{cases} 0, & x < -\varepsilon, \\ (2\varepsilon + 6t)^{-1}(x + \varepsilon), & -\varepsilon \le x \le \varepsilon + 6t, \\ 1, & x > \varepsilon + 6t. \end{cases}$$

Location $\xi(t)$ of the solitary wave on the RW is detected numerically from which we determine

$$a^2(t) = (2\varepsilon + 6t)^{-1}(\xi(t) + \varepsilon) \quad \text{as long as} \quad \xi(t) \in [-\varepsilon, \varepsilon + 6t].$$

This gives the theoretical prediction of the amplitude of the solitary wave,

$$A(t) = 2\mu_0^2 - a^2(t).$$

The theoretical prediction can be compared with the numerical approximation of the amplitude of the solitary wave computed by the quadratic interpolation from three grid points near the maximum of u.

Figure 2.5 shows the numerically detected amplitude of the solitary wave versus time (left) and versus the amplitude of the RW background (right) for the transmitted soliton with $\mu_0 = 1.4 > c = 1$. The numerical approximation is shown by black dots. The red dots show the final amplitude $A_\infty = 2\mu_0^2 - c^2$ (left) and the theoretically computed amplitude $A(t) = 2\mu_0^2 - a^2(t)$ (right). It is obvious that the discrepancy between black and red dots disappear with time and that $A(t) \to A_\infty$ as t evolves. The blue line on the right panel shows the amplitude of the background $a^2(t)$ at the location of the transmitted soliton. Since $a^2(t) \to c^2$ and $A_\infty > c^2$ since $\mu_0 = 1.4 > c = 1$, the black and blue lines do not meet and the soliton is transmitted over the RW background as seen in Figure 2.2.

Figure 2.6 shows the same quantities as Figure 2.5 but for the trapped soliton with $\mu_0 = 0.95 < c = 1$. Since $A_\infty = 2\mu_0^2 - c^2 < c^2$, the amplitude of the solitary wave never reaches the horizontal asymptote on the left panel because the trapped soiton dissolves inside the RW. The right panel shows again that the numerical approximation (black dots) is getting closer to the theoretical approximation of the soliton amplitude $A(t)$ (red dots) as t evolves. However, for the trapped soliton the black and blue lines meet so that there exists the limiting value of the background a_∞^2 such that $a(t) \to a_\infty$ as $t \to \infty$. The limiting value a_∞ is found from the balance $2\mu_0^2 - a_\infty^2 = a_\infty^2$ at $a_\infty = \mu_0$. Hence, the trapped solitary wave completely disappears inside the RW background as seen in Figure 2.3.

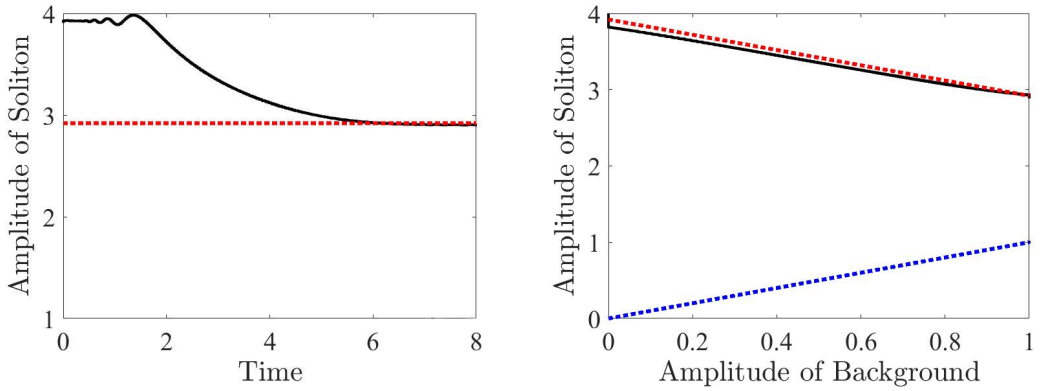

(A) (B)

FIGURE 2.5: Data analysis for the transmitted soliton shown in Figure 2.2: (a) Amplitude of the solitary wave versus time (black) and the limiting amplitude $A_\infty = 2\mu_0^2 - c^2$ (red). (b) Amplitude of the solitary wave versus amplitude of the RW background detected numerically (black) and theoretically (red). The blue dots show the amplitude of the RW background.

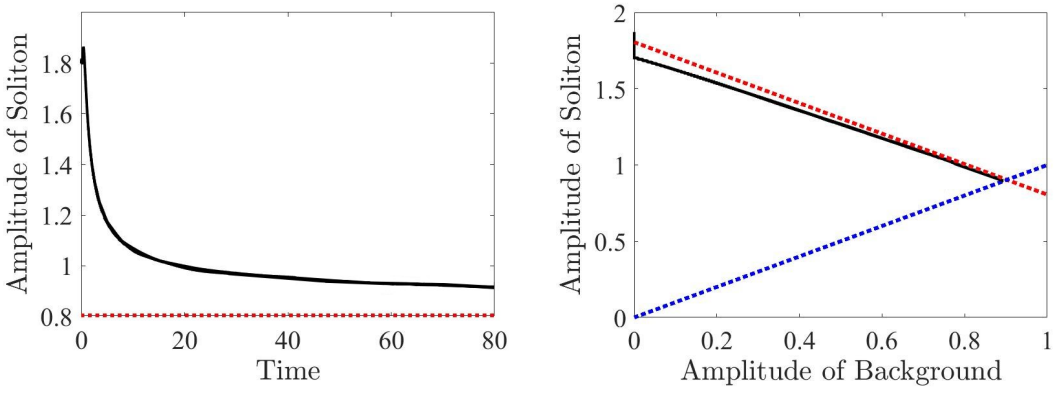

(A) (B)

FIGURE 2.6: The same as Figure 2.5 but for the trapped soliton shown in Figure 2.3.

Chapter 3

Solitons on the Cnoidal Wave Background

We consider an important related problem in the DSW theory, which is describing solitons interaction with a cnoidal wave background. The main focus of this chapter is construction and analysis of exact solutions for these interactions.

Compared to the previous works, which involve Weierstrass functions with complex translation parameters, our solutions expressed in terms of Jacobi elliptic functions have real-valued parameters, which allows us to clarify the dynamic nature of soliton-cnoidal wave interactions, and to characterize their corresponding properties.

We also demonstrate that the Darboux transformation provides a more straightforward method for obtaining these complicated interaction solutions compared to the degeneration methods mentioned in Chapter 1.

Due to the unsteady, wavepacket-like character of the soliton-cnoidal wave interaction solutions, such wave patterns are referred to as breathers. Breathers generalize classical solitons by incorporating time scale associated with internal oscillations, in addition to the one associated with propagation. In this chapter we obtain both families of breather solutions, namely the elevation (bright) and depression (dark) breather solutions. Both the solution families are determined by two distinct parameters, which are initial position and a spectral parameter. The nonlinear dispersion relations demonstrate that the bright (dark) breathers propagate faster (slower) than the cnoidal wave background.

These results provide insight into recent experiments on soliton-cnoidal wave collisions. Mao et. al [37] recently showed that the class of breathers considered in this Chapter,

can be interpreted as a nonlinear superposition between a soliton and a cnoidal wave, by constructing experimentally and numerically strongly nonlinear, topological breathers through an interaction of a carrier wave with a soliton or vice-versa. Thus, the exact solutions for soliton-cnoidal wave interactions derived in this Chapter served as a guiding insight for the experimental and numerical work in [37].

3.1 Traveling cnoidal wave

A traveling wave solution $u(x,t) = \phi(x - ct)$ to the KdV equation (1.1) satisfies the second-order equation after integration in x:

$$\phi'' + 3\phi^2 - c\phi = b, \tag{3.1}$$

where $b \in \mathbb{R}$ is the integration constant and the single variable x stands for $x - ct$. The second-order equation (3.1) is integrable with the first-order invariant

$$(\phi')^2 + 2\phi^3 - c\phi^2 - 2b\phi = d, \tag{3.2}$$

where $d \in \mathbb{R}$ is another integration constant. The following (well-known) proposition summarizes the existence of periodic solutions to system (3.1) and (3.2).

Proposition 3.1. *There exists a family of periodic solutions to system (3.1) and (3.2) for every (b,c,d) satisfying $c^2 + 12b > 0$ and $d \in (U(\phi_+), U(\phi_-))$, where $U(\phi) := 2\phi^3 - c\phi^2 - 2b\phi$ and $\phi_\pm$ are critical points of U given by $\phi_\pm = (c \pm \sqrt{c^2 + 12b})/6$.*

Proof. If $c^2 + 12b > 0$, the mapping $\phi \mapsto U(\phi)$ has two critical points $\phi_\pm$. Since $U'(\phi_\pm) = 6\phi_\pm^2 - 2c\phi_\pm - 2b = 0$ and $U''(\phi_\pm) = 12\phi_\pm - 2c = \pm 2\sqrt{c^2 + 12b}$, ϕ_+ is the minimum of U and ϕ_- is the maximum of U. If $d = U(\phi_+)$, the only bounded solution of system (3.1) and (3.2) is a constant solution corresponding to the center point $(\phi_+, 0)$. If $d = U(\phi_-)$, the only bounded solution of system (3.1) and (3.2) is a homoclinic orbit from the saddle point $(\phi_-, 0)$ which surrounds the center point $(\phi_+, 0)$. The family of periodic orbits exists in a punctured neighbourhood around the center point enclosed by the homoclinic orbit, for $d \in (U(\phi_+), U(\phi_-))$.

If $c^2 + 12b \leq 0$, the mapping $\phi \mapsto U(\phi)$ is monotonically increasing. There exist no bounded solutions of system (3.1) and (3.2) with the exception of the constant solution $\phi = c/6$ in the marginal case $c^2 + 12b = 0$. □

It follows from Proposition 3.1 that the most general traveling periodic wave solution has three parameters (b, c, d) that are defined in a subset of $\mathbb{R}^3$ for which $c^2 + 12b > 0$ and $d \in U(\phi_+), U(\phi_-))$. For each (b, c, d) in this subset of $\mathbb{R}^3$, the translational parameter $x_0 \in \mathbb{R}$ generates the family of solutions $\phi(x + x_0)$ due to translation symmetry.

The two parameters of the family of periodic solutions can be set uniquely due to the following two symmetries:

Definition 3.2. The KdV equation (1.1) is invariant under the **scaling transformation**: if $u(x, t)$ is a solution, then so is $\alpha^2 u(\alpha x, \alpha^3 t)$, $\alpha > 0$.

Definition 3.3. The KdV equation (1.1) is invariant under the **Galilean transformation**: if $u(x, t)$ is a solution, then so is $\beta + u(x - 6\beta t, t)$, $\beta \in \mathbb{R}$.

Due to these symmetries, if ϕ_0 is a periodic solution to system (3.1) and (3.2) with $(b, c, d) = (b_0, c_0, d_0)$, then $\beta + \alpha^2 \phi_0(\alpha x)$ is also a periodic solution to system (3.1) and (3.2) with

$$(b, c, d) = (-3\beta^2 - \alpha^2 \beta c_0 + \alpha^4 b_0, 6\beta + \alpha^2 c_0, 2\beta^3 + \alpha^2 \beta^2 c_0 - 2\beta \alpha^4 b_0 + \alpha^6 d_0),$$

where $\alpha > 0$ and $\beta \in \mathbb{R}$ are arbitrary parameters. The constant in Proposition 3.1 is invariant under the transformation since $c^2 + 12b = \alpha^4 (c_0^2 + 12 b_0) > 0$. Thus, without loss of generality, we can consider the normalized travelling cnoidal traveling wave

$$u(x, t) = \phi_0(x - c_0 t), \quad \phi_0(x) = 2k^2 \mathrm{cn}^2(x, k) \tag{3.3}$$

for which the values of (b_0, c_0, d_0) are determined in the following proposition.

Proposition 3.4. *The normalized cnoidal wave $\phi_0(x) = 2k^2 \mathrm{cn}^2(x, k)$ is a periodic solution of system (3.1) and (3.2) for*

$$b_0 := 4k^2(1 - k^2), \quad c_0 := 4(2k^2 - 1), \quad d_0 = 0,$$

where $k \in (0, 1)$ is an arbitrary parameter.

Proof. Since $\min\limits_{x \in \mathbb{R}} \phi_0(x) = 0$, it follows from (3.2) that $d_0 = U(0) = 0$. On the other hand, by using the fundamental relations on the Jacobi elliptic functions (3.15) and the relations for their derivatives (A.2) included in the Appendix A, we obtain from (3.2) with $d_0 = 0$ that $b_0 = 4k^2(1 - k^2)$ and $c_0 = 4(2k^2 - 1)$. □

3.2 Lamé equation as the spectral problem

The spectral problem (1.2) with the normalized cnoidal wave (3.3) as the potential u is known as the Lamé equation [30, p.395]. It can be written in the form

$$v''(x) - 2k^2\mathrm{sn}^2(x,k)v(x) + \eta v(x) = 0, \quad \eta := \lambda + 2k^2, \tag{3.4}$$

where the single variable x stands for $x - c_0 t$. By using (A.1) and (A.2), we obtain the following three particular solutions $v = v_{1,2,3}(x)$ of the Lamé equation (3.4) with the corresponding spectral parameters $\lambda = \lambda_{1,2,3}(k)$:

$$\begin{aligned} \lambda_1(k) &:= -k^2, & v_1(x) &:= \mathrm{dn}(x,k), \\ \lambda_2(k) &:= 1 - 2k^2, & v_2(x) &:= \mathrm{cn}(x,k), \\ \lambda_3(k) &:= 1 - k^2, & v_3(x) &:= \mathrm{sn}(x,k), \end{aligned}$$

which correspond to the three remarkable values of η: $\eta_1 = k^2$, $\eta_2 = 1$, and $\eta_3 = 1 + k^2$. For $k \in (0,1)$, the three eigenvalues are sorted as $\lambda_1(k) < \lambda_2(k) < \lambda_3(k)$.

Figure 3.1 shows the Floquet spectrum of the Lamé equation (3.4) which correspond to the admissible values of λ for which $v \in L^\infty(\mathbb{R})$. The bands are shaded and the band edges shown by the bold solid curves correspond to $\lambda = \lambda_{1,2,3}(k)$ for $k \in (0,1)$. The cnoidal wave is the periodic potential with a single finite gap (the so-called the *one-zone* potential) [42] so that the Floquet spectrum consists of a single finite band $[\lambda_1(k), \lambda_2(k)]$ and the semi-infinite band $[\lambda_3(k), \infty)$.

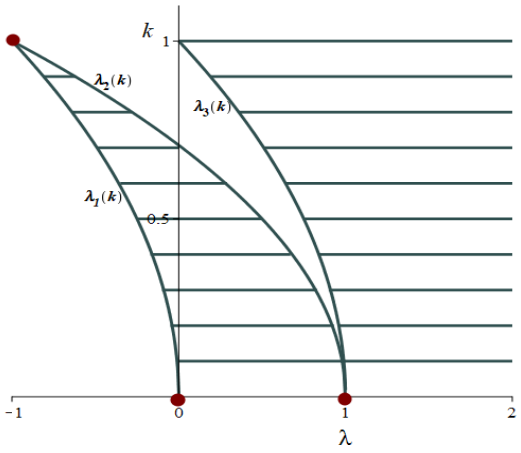

FIGURE 3.1: Floquet spectrum of the Lamé equation (3.4) for different values of $k \in (0,1)$.

As is well-known (see [30, p. 395]), the two linearly independent solutions of the Lamé equation (3.4) for $\lambda \neq \lambda_{1,2,3}(k)$ are given by the functions

$$v_{\pm}(x) = \frac{H(x \pm \alpha)}{\Theta(x)} e^{\mp x Z(\alpha)}, \tag{3.5}$$

where $\alpha \in \mathbb{C}$ is found from $\lambda \in \mathbb{R}$ by using the characteristic equation $\eta = k^2 + \mathrm{dn}^2(\alpha, k)$ and the Jacobi zeta function is $Z(\alpha) := \frac{\Theta'(\alpha)}{\Theta(\alpha)}$, see Table A.1.

Since $\eta = \lambda + 2k^2$, the characteristic equation can be written in the form

$$\lambda = 1 - 2k^2 + k^2 \mathrm{cn}^2(\alpha, k). \tag{3.6}$$

The following proposition clarifies how α is defined from the characteristic equation (3.6) when λ is decreased from $\lambda_3(k)$ to $-\infty$. Figure 3.2 illustrates the path of α in the complex plane.

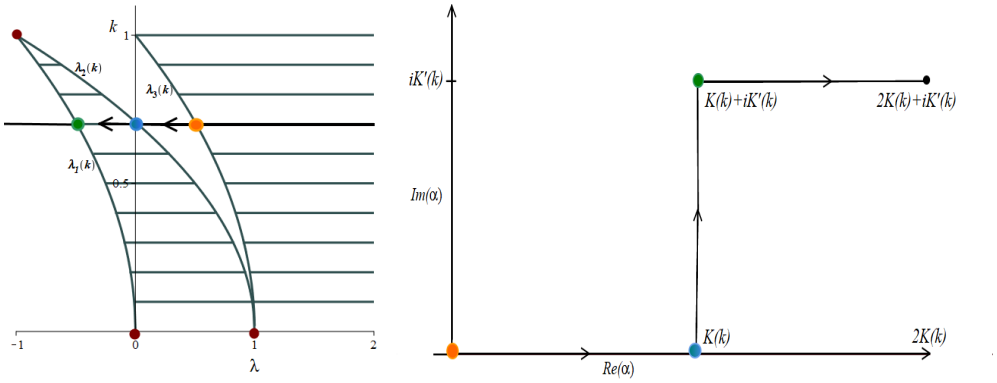

FIGURE 3.2: Left: Floquet spectrum with orange, blue, and green dots corresponding to $\lambda_3(k)$, $\lambda_2(k)$, and $\lambda_1(k)$ for a fixed value of $k \in (0, 1)$. Right: The complex plane for the parameter α indicating the path of α relative to the path of λ.

Proposition 3.5. *Fix $k \in (0, 1)$. We have*

- $\alpha = F(\varphi_\alpha, k) \in [0, K(k)]$ *for* $\lambda \in [\lambda_2(k), \lambda_3(k)]$, *where* $\varphi_\alpha \in [0, \frac{\pi}{2}]$ *is given by*

$$\sin \varphi_\alpha = \frac{\sqrt{1 - k^2 - \lambda}}{k}. \tag{3.7}$$

- $\alpha = K(k) + i\beta$ *with* $\beta = F(\varphi_\beta, k') \in [0, K'(k)]$ *for* $\lambda \in [\lambda_1(k), \lambda_2(k)]$, *where* $\varphi_\beta \in [0, \frac{\pi}{2}]$ *is given by*

$$\sin \varphi_\beta = \frac{\sqrt{1 - 2k^2 - \lambda}}{\sqrt{(1 - k^2)(1 - k^2 - \lambda)}}. \tag{3.8}$$

- $\alpha = K(k) + iK'(k) + \gamma$ *with* $\gamma = F(\varphi_\gamma, k) \in [0, K(k))$ *for* $\lambda \in (-\infty, \lambda_1(k)]$, *where* $\varphi_\gamma \in [0, \frac{\pi}{2})$ *is given by*

$$\sin\varphi_\gamma = \frac{\sqrt{-k^2-\lambda}}{\sqrt{1-2k^2-\lambda}}, \tag{3.9}$$

where $k' = \sqrt{1-k^2}$ *and* $K'(k) = K(k')$.

Proof. When $\lambda \in [\lambda_2(k), \lambda_3(k)]$, it follows from (3.6) that $\mathrm{cn}^2(\alpha, k) \in [0, 1]$ and hence $\alpha \in [0, K(k)]$ mod$K(k)$. Solving (3.6) in $\sin\varphi_\alpha = \mathrm{sn}(\alpha, k)$ yields (3.7). As λ is decreased from $\lambda_3(k)$ to $\lambda_2(k)$, φ_α is monotone increasing and so is $F(\varphi_\alpha, k)$. Hence, α increases from 0 to $K(k)$. See the orange and blue dots in Figure 3.2.

When $\lambda \in [\lambda_1(k), \lambda_2(k)]$, we use the special relations (see [26, 8.151 and 8.153]),

$$\mathrm{cn}(K(k) + i\beta, k) = -k'\frac{\mathrm{sn}(i\beta, k)}{\mathrm{dn}(i\beta, k)} = -ik'\frac{\mathrm{sn}(\beta, k')}{\mathrm{dn}(\beta, k')},$$

where $k' := \sqrt{1-k^2}$. The characteristic equation (3.6) is rewritten in the form

$$\mathrm{sn}^2(\beta, k') = \frac{1-2k^2-\lambda}{(1-k^2)(1-k^2-\lambda)},$$

from which it follows that $\mathrm{sn}^2(\beta, k') \in [0, 1]$ and hence $\beta \in [0, K(k')]$ mod$K(k')$. Solving in $\sin\varphi_\beta = \mathrm{sn}(\beta, k')$ yields (3.8). When λ is decreased from $\lambda_2(k)$ to $\lambda_1(k)$, then φ_β is monotone increasing and so is $F(\varphi_\beta, k')$. Hence, β increases from 0 to $K'(k)$. See blue and green dots on Figure 3.2.

When $\lambda \in (-\infty, \lambda_1(k)]$, we use the special relations (see [26, 8.151]),

$$\mathrm{cn}(K(k) + iK'(k) + \gamma) = -\frac{ik'}{k\mathrm{cn}(\gamma, k)},$$

and rewrite the characteristic equation (3.6) in the form

$$\mathrm{cn}^2(\gamma, k) = \frac{1-k^2}{1-2k^2-\lambda}.$$

from which it follows that $\mathrm{cn}^2(\gamma, k) \in [0, 1]$ and hence $\gamma \in [0, K(k))$ mod$K(k)$. Solving in $\sin\varphi_\gamma = \mathrm{sn}(\gamma, k)$ yields (3.9). When λ is decreased from $\lambda_1(k)$ to $-\infty$, then φ_γ is monotone increasing and so is $F(\varphi_\gamma, k)$. Hence, γ increases from 0 to $K(k)$. See the green and black dots in Figure 3.2. □

3.3 Time evolution of the eigenfunctions

Let $u(x,t) = \phi_0(x - c_0 t)$ be the normalized cnoidal wave (3.3) and $v(x,t) = v_\pm(x,t)$ be a solution of system (1.2) and (1.3) such that $v_\pm(x,0) = v_\pm(x)$ is given by (3.5). The time dependence of $v_\pm(x,t)$ can be found by the separation of variables:

$$v_\pm(x,t) = \frac{H(x - c_0 t \pm \alpha)}{\Theta(x - c_0 t)} e^{\mp(x - c_0 t) Z(\alpha) \mp t\omega(\alpha)}, \tag{3.10}$$

where $\omega(\alpha)$ is to be found. After substituting (3.10) into (1.3) and dividing by $v_\pm(x,t)$, we obtain

$$\omega(\alpha) = (c_0 + 4\lambda - 2\phi_0(x)) \left[Z(\alpha) \pm Z(x) \mp \frac{H'(x \pm \alpha)}{H(x \pm \alpha)} \right] \mp \phi_0'(x), \tag{3.11}$$

where x stands again for $x - ct$. Equation (3.11) holds for every $x \in \mathbb{R}$ due to compatibility of system (1.2) and (1.3). Hence, we obtain $\omega(\alpha)$ by substituting $c_0 = 4(2k^2 - 1)$ and evaluating (3.11) at $x = 0$:

$$\omega(\alpha) = 4(\lambda + k^2 - 1) \left[\frac{\Theta'(\alpha)}{\Theta(\alpha)} - \frac{H'(\alpha)}{H(\alpha)} \right], \tag{3.12}$$

where we have used the parity properties [26, 8.192]:

$$H(-x) = -H(x) \qquad \text{and} \qquad \Theta(-x) = \Theta(x).$$

The following proposition ensures that $\omega(\alpha)$ is real when λ is taken either in the semi-infinite gap $(-\infty, \lambda_1(k))$ or in the finite gap $(\lambda_2(k), \lambda_3(k))$.

Proposition 3.6. *Fix $k \in (0,1)$. Then, $\omega(\alpha) \in \mathbb{R}$ if $\lambda \in (-\infty, \lambda_1(k)) \cup (\lambda_2(k), \lambda_3(k))$ and $\omega(\alpha) \in i\mathbb{R}$ if $\lambda \in [\lambda_1(k), \lambda_2(k)]$.*

Proof. We recall the logarithmic derivatives of the Jacobi theta functions [26, 8.199(3)]:

$$\frac{H'(x)}{H(x)} = \frac{\pi}{2K(k)}\left[\cot\left(\frac{\pi x}{2K(k)}\right) + 4\sin\left(\frac{\pi x}{K(k)}\right)\sum_{n=1}^{\infty}\frac{q^{2n}}{1-2q^{2n}\cos\left(\frac{\pi x}{K(k)}\right)+q^{4n}}\right],$$
$$\frac{H_1'(x)}{H_1(x)} = -\frac{\pi}{2K(k)}\left[\tan\left(\frac{\pi x}{2K(k)}\right) + 4\sin\left(\frac{\pi x}{K(k)}\right)\sum_{n=1}^{\infty}\frac{q^{2n}}{1+2q^{2n}\cos\left(\frac{\pi x}{K(k)}\right)+q^{4n}}\right],$$
$$\frac{\Theta_1'(x)}{\Theta_1(x)} = -\frac{2\pi}{K(k)}\sin\left(\frac{\pi x}{K(k)}\right)\sum_{n=1}^{\infty}\frac{q^{2n-1}}{1+2q^{2n}\cos\left(\frac{\pi x}{K(k)}\right)+q^{4n-2}},$$
$$\frac{\Theta'(x)}{\Theta(x)} = \frac{2\pi}{K(k)}\sin\left(\frac{\pi x}{K(k)}\right)\sum_{n=1}^{\infty}\frac{q^{2n-1}}{1-2q^{2n}\cos\left(\frac{\pi x}{K(k)}\right)+q^{4n-2}},$$

where $q := e^{-\frac{\pi K'(k)}{K(k)}}$ is the Jacobi nome, see Table A.1.

If $\lambda \in [\lambda_2(k), \lambda_3(k)]$, then $\alpha = F(\varphi_\alpha, k) \in [0, K(k)]$ by Proposition 3.5 and (3.12) returns real $\omega(\alpha)$, where both logarithmic derivatives of the Jacobi theta functions are positive.

If $\lambda \in [\lambda_1(k), \lambda_2(k)]$, then $\alpha = K(k)+i\beta$ with $\beta = F(\varphi_\beta, k') \in [0, K'(k)]$ by Proposition 3.5. The half-period translations [26, 8.183] yield

$$H(K(k)+i\beta) = H_1(i\beta),$$
$$\Theta(K(k)+i\beta) = \Theta_1(i\beta),$$

so that the logarthmic derivatives in (3.12) are purely imaginary and $\omega(K(k)+i\beta) \in i\mathbb{R}$.

If $\lambda \in (-\infty, \lambda_1(k)]$, then $\alpha = K(k) + iK'(k) + \gamma$ with $\gamma = F(\varphi_\gamma, k) \in [0, K(k))$ by Proposition 3.5. The half-period translations [26, 8.183] yield

$$H(K(k)+iK'(k)+\gamma) = e^{\frac{\pi K'(k)}{4K(k)}}e^{-\frac{i\pi\gamma}{2K(k)}}\Theta_1(\gamma),$$
$$\Theta(K(k)+iK'(k)+\gamma) = e^{\frac{\pi K'(k)}{4K(k)}}e^{-\frac{i\pi\gamma}{2K(k)}}H_1(\gamma),$$

The purely imaginary part of the logarithmic derivatives cancels in (3.12) after the transformation and we obtain the real quantity

$$\omega(K(k)+iK'(k)+\gamma) = 4(\lambda+k^2-1)\left[\frac{H_1'(\gamma)}{H_1(\gamma)} - \frac{\Theta_1'(\gamma)}{\Theta_1(\gamma)}\right], \tag{3.13}$$

where both logarithmic derivatives are negative. □

3.4 New solutions via the Darboux transformation

By now, the readers should be familiar with the method of constructing new solution using the Darboux Transformation. Following the methodology presented in Section 1.4 and Section 2.4, here we fix a value of $\lambda = \lambda_0$ and obtain a solution $v = v_0(x,t)$ of the linear equations (1.2) and (1.3) associated with the potential $u = \phi_0(x - c_0 t)$ of the KdV equation (1.1). Thus, the formula for the Darboux Transformation (1.5) becomes

$$\hat{u}(x,t) = \phi_0(x - c_0 t) + 2\partial_x^2 \log v_0(x,t). \tag{3.14}$$

- The new solution $\hat{u}$ is nonsingular for $\lambda_0 \in (-\infty, \lambda_1(k))$, which is below the Floquet spectrum (Figure 3.1). This is because Sturm's nodal theorem implies that $v_\pm(x,t)$, given by (3.10), are sign-definite in x for every $t \in \mathbb{R}$, and thus $v_0(x,t) \neq 0$ everywhere.
- If $\lambda_0 \in (\lambda_2(k), \lambda_3(k))$ is in the finite gap, Sturm's nodal theorem implies that $v_\pm(x,t)$ have exactly one zero on the fundamental period of ϕ_0 for every $t \in \mathbb{R}$. We will show that this technical obstacle can be overcome with the translation of the new solution $\hat{u}(x,t)$ with respect to a half-period in the complex plane of x.

Before we proceed with the construction of the new solutions, we need to connect $\phi_0(x - c_0 t)$ given by (3.3) with the Jacobi theta function used to represent v_0. The following proposition gives an important relation between the Jacobi cnoidal function and the Jacobi theta function.

Proposition 3.7. *For every $k \in (0,1)$, we have*

$$k^2 \mathrm{cn}^2(x,k) = k^2 - 1 + \frac{E(k)}{K(k)} + \partial_x^2 \log \Theta(x). \tag{3.15}$$

Proof. It follows from [32, equation (3.5.1)] that

$$\partial_y^2 \log \theta_4(y) = \frac{\theta_4''(0)}{\theta_4(0)} - \theta_2^4(0)\mathrm{sn}^2(x,k),$$

where

$$y = \frac{x}{\theta_3^2(0)} = \frac{\pi x}{2K(k)} \quad \text{and} \quad k = \frac{\theta_2^2(0)}{\theta_3^2(0)}.$$

This yields with the chain rule that

$$\partial_x^2 \log \Theta(x) = \frac{\Theta''(0)}{\Theta(0)} - k^2 \mathrm{sn}^2(x,k).$$

Since $\mathrm{sn}^2(x,k) = 1 - \mathrm{cn}^2(x,k)$ and

$$\frac{\Theta''(0)}{\Theta(0)} = 1 - \frac{E(k)}{K(k)}$$

by using [26, 8.196], we obtain (3.15). □

This brings us to the main result of this work; which is the derivation and analysis of two solution families of the KdV equation (1.1) parametrized by λ and $x_0 \in \mathbb{R}$, where λ belongs to $(-\infty, -k^2)$ for the bright breather family and $(1-2k^2, 1-k^2)$ for the dark breather family. The two solution families are discussed in full detail in the next two subsections.

3.4.1 Bright Breather on the Cnoidal Wave Background

The following theorem presents the construction of bright breathers via the Darboux transformation (3.14).

Theorem 3.8. *There exists an exact solution to the KdV equation (1.1) in the form*

$$u(x,t) = 2\left[k^2 - 1 + \frac{E(k)}{K(k)}\right] + 2\partial_x^2 \log \tau(x,t), \tag{3.16}$$

where the τ-function is given by

$$\tau(x,t) := \Theta(x - c_0 t + \alpha_b) e^{\kappa_b (x - c_b t + x_0)} + \Theta(x - c_0 t - \alpha_b) e^{-\kappa_b (x - c_b t + x_0)}, \tag{3.17}$$

where $x_0 \in \mathbb{R}$ is arbitrary and $\alpha_b \in (0, K(k))$, $\kappa_b > 0$, and $c_b > c_0$ are uniquely defined from $\lambda \in (-\infty, \lambda_1(k))$ by

$$\alpha_b = F(\varphi_\gamma, k), \tag{3.18}$$

$$\kappa_b = \frac{\sqrt{1-\lambda-k^2}\sqrt{-\lambda-k^2}}{\sqrt{1-2k^2-\lambda}} - Z(\varphi_\gamma, k), \tag{3.19}$$

$$c_b = c_0 + \frac{4\sqrt{1-\lambda-2k^2}\sqrt{1-\lambda-k^2}\sqrt{-\lambda-k^2}}{\kappa_b}, \tag{3.20}$$

where $\varphi_\gamma \in (0, \frac{\pi}{2})$ is found from

$$\sin\varphi_\gamma = \frac{\sqrt{-\lambda-k^2}}{\sqrt{1-2k^2-\lambda}}. \tag{3.21}$$

Proof. Consider a linear combination of the two solutions to the linear system (1.2) and (1.3) in the form (3.10) with $\alpha = K(k) + iK'(k) + \gamma$ and $\gamma = F(\varphi_\gamma, k) \in (0, K(k))$:

$$v_0(x,t) = c_+ \frac{H(x - c_0 t + \alpha)}{\Theta(x - c_0 t)} e^{-(x-c_0 t)Z(\alpha) - \omega(\alpha)t} + c_- \frac{H(x - c_0 t - \alpha)}{\Theta(x - c_0 t)} e^{+(x-c_0 t)Z(\alpha) + \omega(\alpha)t}, \tag{3.22}$$

where (c_+, c_-) are arbitary constants. By using the half-period translations of the Jacobi theta functions [26, 8.183], we obtain for $\alpha = K(k) + iK'(k) + \gamma$:

$$\begin{aligned} H(x+\alpha) &= e^{\frac{\pi K'(k)}{4K(k)} - \frac{i\pi(x+\gamma)}{2K(k)}} \Theta(x + K(k) + \gamma), \\ H(x-\alpha) &= -e^{\frac{\pi K'(k)}{4K(k)} + \frac{i\pi(x-\gamma)}{2K(k)}} \Theta(x + K(k) - \gamma), \end{aligned}$$

and

$$Z(\alpha) = \frac{H_1'(\gamma)}{H_1(\gamma)} - \frac{i\pi}{2K(k)}.$$

Substituting these expressions into (3.22) cancels the x-dependent complex phases. Anticipating (3.14), we set

$$c_+ = c e^{-(K(k)+x_0)\frac{H_1'(\gamma)}{H_1(\gamma)}}, \quad c_- = -c e^{(K(k)+x_0)\frac{H_1'(\gamma)}{H_1(\gamma)}}$$

with arbitrary parameters $c, x_0 \in \mathbb{R}$, from which the constant c cancels out due to the second logarithmic derivative. Using $c_\pm$ in (3.22), inserting v_0 into (3.14), and simplifying with the help of (3.15), we obtain a new solution in the final form $u(x,t) := \hat{u}(x - K(k), t)$, where $u(x,t)$ is given by (3.16) with $\tau(x,t)$ given by (3.17) with the following parameters: $\alpha_b := \gamma \in (0, K(k))$, $\kappa_b := -\frac{H_1'(\gamma)}{H_1(\gamma)} > 0$, and

$$\begin{aligned} c_b &:= c_0 - \omega(K(k) + iK'(k) + \gamma)\frac{H_1(\gamma)}{H_1'(\gamma)} \\ &= 4(k^2 - \lambda) + 4(\lambda + k^2 - 1)\frac{\Theta_1'(\gamma) H_1(\gamma)}{\Theta_1(\gamma) H_1'(\gamma)}, \end{aligned}$$

where we have used (3.13). By using the following identities [11, 1053.02]

$$\begin{aligned} \frac{H_1'(\gamma)}{H_1(\gamma)} &= -\frac{\mathrm{sn}(\gamma,k)\mathrm{dn}(\gamma,k)}{\mathrm{cn}(\gamma,k)} + Z(\gamma), \\ \frac{\Theta_1'(\gamma)}{\Theta_1(\gamma)} &= -\frac{k^2 \mathrm{sn}(\gamma,k)\mathrm{cn}(\gamma,k)}{\mathrm{dn}(\gamma,k)} + Z(\gamma), \end{aligned}$$

and the relation formulas $Z(\gamma) = Z(\varphi_\gamma, k)$,

$$\mathrm{sn}(\gamma, k) = \sin(\varphi_\gamma) = \frac{\sqrt{-\lambda - k^2}}{\sqrt{1 - 2k^2 - \lambda}}, \quad \mathrm{cn}(\gamma, k) = \cos(\varphi_\gamma) = \frac{\sqrt{1 - k^2}}{\sqrt{1 - 2k^2 - \lambda}},$$

and

$$\mathrm{dn}(\gamma, k) = \frac{\sqrt{1 - k^2}\sqrt{1 - \lambda - k^2}}{\sqrt{1 - 2k^2 - \lambda}},$$

we express parameters α_b, κ_b, and c_b in terms of incomplete elliptic integrals in (3.18), (3.19), and (3.20). Since $\kappa_b > 0$, it follows that $c_b > c_0$. □

Remark 3.9. The solution $u(x,t)$ obtained in the proof of Theorem 3.8 is the half-period translation along the real axis of the solution $\hat{u}(x,t)$ defined by (3.14).

Remark 3.10. Since $\kappa_b > 0$, it follows from (3.16), (3.17), and (3.15) that

$$u(x,t) \to 2k^2 \mathrm{cn}^2(x - c_0 t \pm \alpha_b, k) \quad \text{as} \quad x - c_b t \to \pm\infty.$$

A suitably normalized phase shift of the background cnoidal wave can be written in the form:

$$\Delta_b := -\frac{2\pi\alpha_b}{K(k)} = -\frac{2\pi F(\varphi_\gamma, k)}{K(k)} \in (-2\pi, 0).$$

When $\Delta_b \in (-\pi, 0)$, the normalized phase shift is negative. When $\Delta_b \in (-2\pi, \pi]$, the normalized phase shift is considered to be positive by a period translation to $2\pi + \Delta_b \in (0, \pi)$.

Figure 3.3 depicts the spatiotemporal evolution of a solution $u(x,t)$ given by (3.16) and (3.17). This solution represents a bright breather with speed $c_b > c_0$ and inverse width κ_b propagating through a background cnoidal wave with speed c_0. As a result of the bright soliton, the cnoidal background is spatially shifted by $-2\alpha_b$.

3.4.2 Dark Breather on the Cnoidal Background

The following theorem presents the construction of dark breathers via the Darboux transformation (3.14).

Theorem 3.11. *There exists an exact solution to the KdV equation (1.1) in the form*

$$u(x,t) = 2\left[k^2 - 1 + \frac{E(k)}{K(k)}\right] + 2\partial_x^2 \log \tau(x,t), \tag{3.23}$$

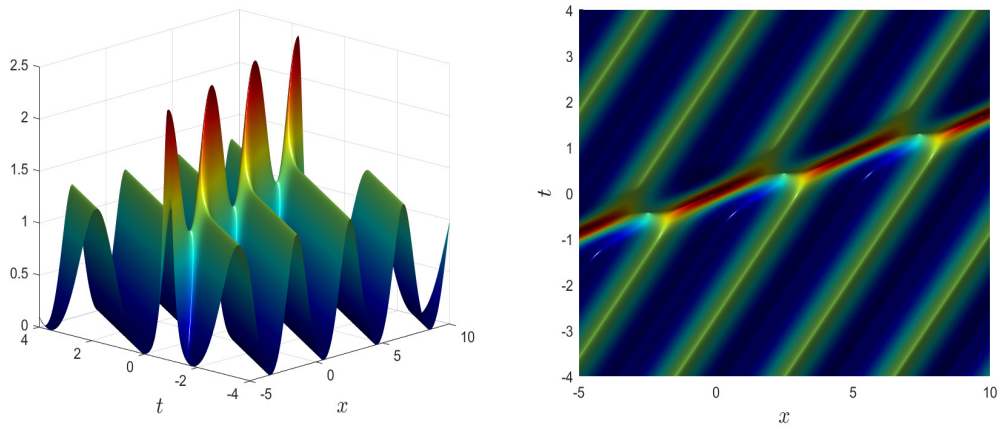

FIGURE 3.3: Bright breather on the cnoidal wave with $k = 0.8$ for $\lambda = -1.2$ and $x_0 = 0$.

where the τ-function is given by

$$\tau(x,t) := \Theta(x - c_0 t + \alpha_d) e^{-\kappa_d (x - c_d t + x_0)} + \Theta(x - c_0 t - \alpha_d) e^{\kappa_d (x - c_d t + x_0)}, \tag{3.24}$$

where $x_0 \in \mathbb{R}$ is arbitrary and $\alpha_d \in (0, K(k))$, $\kappa_d > 0$, and $c_d < c_0$ are uniquely defined from $\lambda \in (\lambda_2(k), \lambda_3(k))$ by

$$\alpha_d = F(\varphi_\alpha, k), \tag{3.25}$$

$$\kappa_d = Z(\varphi_\alpha, k), \tag{3.26}$$

$$c_d = c_0 - \frac{4\sqrt{(k^2+\lambda)(\lambda - 1 + 2k^2)(1 - k^2 - \lambda)}}{\kappa_d}, \tag{3.27}$$

where $\varphi_\alpha \in (0, \frac{\pi}{2})$ is found from

$$\sin \varphi_\alpha = \frac{\sqrt{1 - k^2 - \lambda}}{k}. \tag{3.28}$$

Proof. Consider a linear combination of the form (3.22), but this time with $\alpha = F(\varphi_\alpha, k) \in [0, K(k)]$ for $\lambda \in (\lambda_2(k), \lambda_3(k))$. In this case, $\omega(\alpha)$ and $Z(\alpha) = Z(\varphi_\alpha, k)$ are real by Propositions 3.5 and 3.6. However, functions $H(x \pm \alpha)$ change sign so that we should express them in terms of functions $\Theta(x \pm \alpha)$ after complex translation of phases. This is achieved by the half-period translations [26, 8.183]:

$$H(x+\alpha) = i e^{-\frac{\pi K'(k)}{4K(k)} - \frac{i\pi(x+\alpha)}{2K(k)}} \Theta(x + \alpha - iK'(k)),$$

$$H(x-\alpha) = i e^{-\frac{\pi K'(k)}{4K(k)} - \frac{i\pi(x-\alpha)}{2K(k)}} \Theta(x - \alpha - iK'(k)).$$

The x-dependent complex phase is now a multiplier in the linear superposition (3.22) which does not affect the result due to the second logarithmic derivative. By using (3.14) and (3.15), we set

$$c_+ = ce^{-(x_0 - iK'(k))Z(\alpha) + \frac{i\pi\alpha}{2K(k)}}, \quad c_- = ce^{(x_0 - iK'(k))Z(\alpha) - \frac{i\pi\alpha}{2K(k)}},$$

and obtain a new solution in the final form $u(x,t) := \hat{u}(x + iK'(k), t)$ with the same $u(x,t)$ as in (3.23) and with $\tau(x,t)$ given by (3.24) with the following parameters: $\alpha_d := \alpha \in (0, K(k))$, $\kappa_b := Z(\alpha) > 0$, and

$$\begin{aligned} c_d &= c_0 - \frac{\omega(\alpha)}{Z(\alpha)} \\ &= 4(k^2 - \lambda) + 4(\lambda + k^2 - 1)\frac{\Theta(\alpha)H'(\alpha)}{\Theta'(\alpha)H(\alpha)}, \end{aligned}$$

where we have used (3.12). Using the following identities [11, 1053.02]

$$\begin{aligned} \frac{H'(\alpha)}{H(\alpha)} &= \frac{\mathrm{cn}(\alpha,k)\mathrm{dn}(\alpha,k)}{\mathrm{sn}(\alpha,k)} + Z(\alpha), \\ \frac{\Theta'(\alpha)}{\Theta(\alpha)} &= Z(\alpha), \end{aligned}$$

and the relations $Z(\alpha) = Z(\varphi_\alpha, k)$,

$$\mathrm{sn}(\alpha,k) = \sin(\varphi_\alpha) = \frac{\sqrt{1-\lambda-k^2}}{k}, \quad \mathrm{cn}(\alpha,k) = \cos(\varphi_\alpha) = \frac{\sqrt{\lambda - 1 + 2k^2}}{k},$$

and $\mathrm{dn}(\alpha,k) = \lambda + k^2$, we express parameters α_d, κ_d, and c_d in terms of incomplete elliptic integrals as (3.25), (3.26), and (3.27). Since $\kappa_d > 0$, we have $c_d < c_0$. □

Remark 3.12. The solution $u(x,t)$ obtained in the proof of Theorem 3.11 is the half-period translation along the imaginary axis of the solution $\hat{u}(x,t)$ defined by (3.14).

Remark 3.13. Since $Z(\varphi_\alpha, k) > 0$, it follows from (3.23), (3.24), and (3.15) that

$$u(x,t) \to 2k^2\mathrm{cn}^2(x - c_0 t \mp \alpha_d, k) \quad \text{as} \quad x - c_d t \to \pm\infty.$$

A suitably normalized phase shift of the background cnoidal wave can be written in the form:

$$\Delta_d = \frac{2\pi\alpha_d}{K(k)} = \frac{\pi F(\varphi_\alpha, k)}{K(k)} \in (0, 2\pi). \tag{3.29}$$

When $\Delta_d \in (0, \pi]$, the normalized phase shift is positive. When $\Delta_d \in (\pi, 2\pi)$, the normalized phase shift is considered to be negative by translation to $\Delta_d - 2\pi \in (-\pi, 0)$.

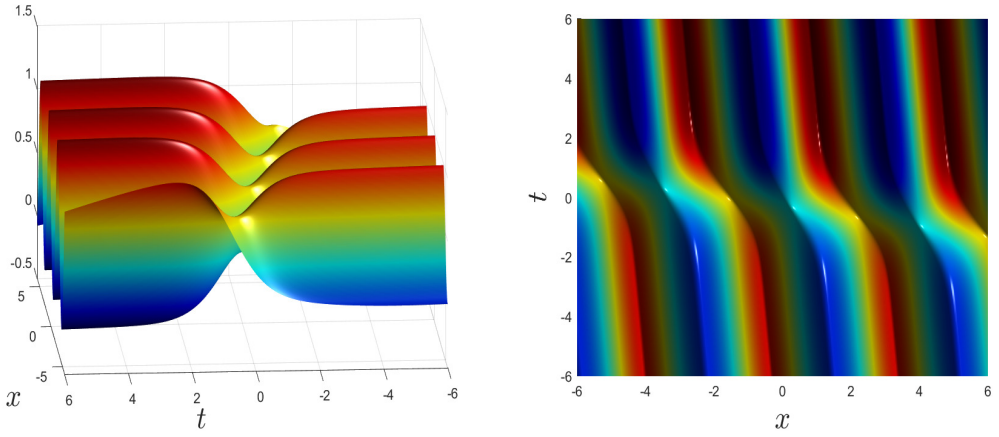

FIGURE 3.4: Dark breather on the cnoidal wave background with $k = 0.7$ for $\lambda = 0.265$ and $x_0 = 0$.

Figure 3.4 shows the spatiotemporal evolution of a solution $u(x,t)$ given by (3.23) and (3.24). This solution resembles a dark breather, where the breather core exhibits the inverse spatial width κ_d and speed $c_d < c_0$ propagating through the cnoidal wave background that has speed c_0. The dark breather gives rise to the translation shift $-2\alpha_d$ of the cnoidal background.

3.5 Properties of the bright breather

Here we exploit the fact that each breather solution is characterized by its position and a spectral parameter, determining a nonlinear dispersion relation, which in turn relates the breather velocity, c, to the breather phase shift, Δ.

Figure 3.5 plots Δ_b, κ_b, and c_b for a bright breather as a function of the parameter λ, see Theorem 3.8 and Remark 3.10. The phase shift Δ_b increases monotonically while the inverse width κ_b and the breather speed c_b decrease monotonically as λ increases from $-\infty$ toward the band edge $\lambda_1(k)$, shown by the vertical dashed line. Since $c_0 = 1.12$ for $k = 0.8$, we confirm that $c_b > c_0$, which can also be observed in Figure 3.3. This characterization is in complete agreement with the experimental and numerical findings in [37], in which they observe a bright breather moving faster than a cnoidal carrier wave, while imparting a topological phase shift.

Figure 3.6 characterizes the family of bright breathers on the background cnoidal wave by plotting $c_b - c_0$ and κ_b versus Δ_b for three values of k. Profiles of breather solutions observed in Figure 3.6 confirm why we call them bright breathers. Bright breathers are

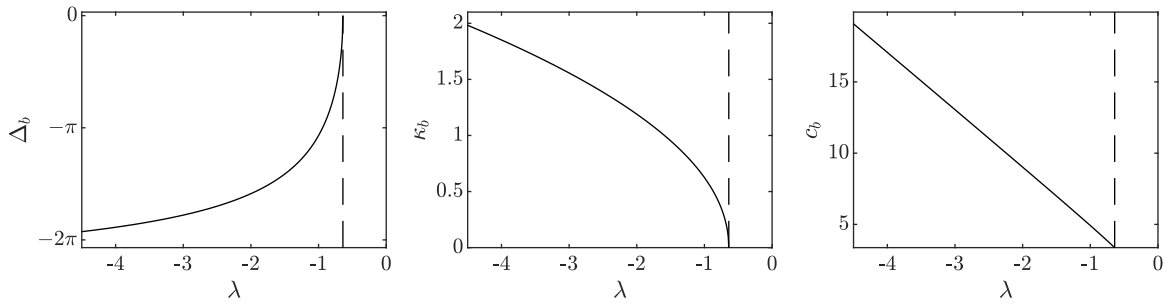

FIGURE 3.5: Normalized phase shift Δ_b (left), inverse width κ_b (middle), and breather speed c_b (right) versus λ in $(-\infty, \lambda_1(k))$ for $k = 0.8$. The band edge $\lambda_1(k) = -k^2$ is shown by the vertical dashed line.

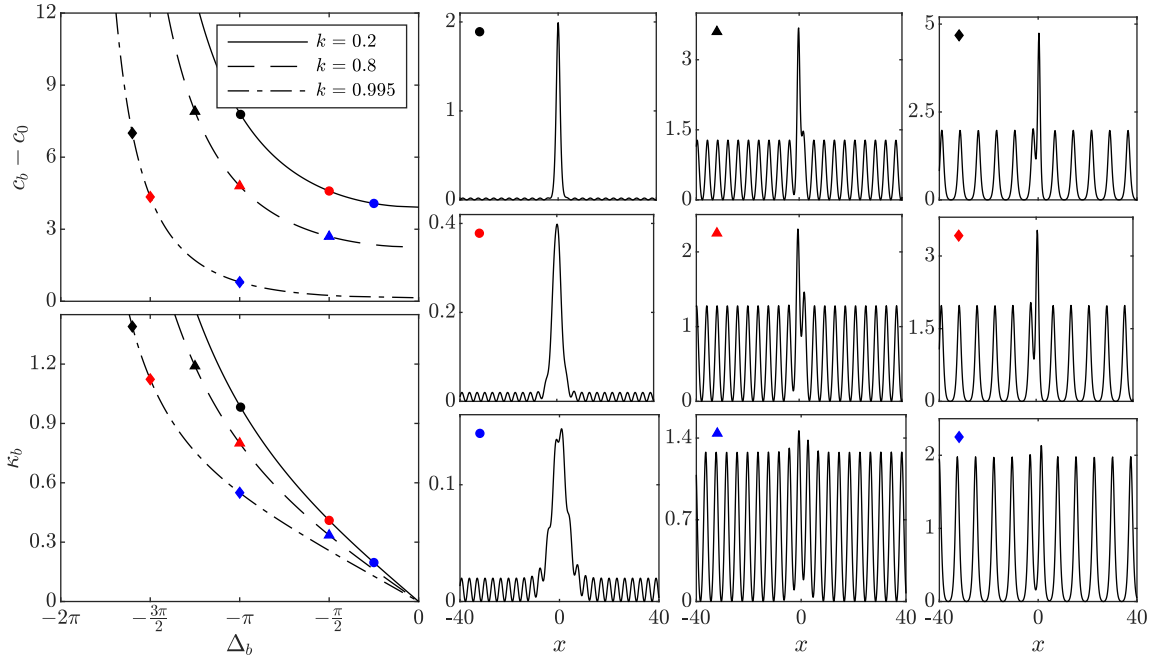

FIGURE 3.6: Left top (bottom): dependence of $c_b - c_0$ (κ_b) versus Δ_b for several values of k. Right: representative solutions for the bright breathers on the background cnoidal waves. Representative solutions are marked on the left panel with a unique colored symbol.

more localized and have larger amplitudes, and move faster for smaller (more negative) values of Δ_b (smaller values of λ). For sufficiently large amplitude, Δ_b falls below $-\pi$ and the breather exhibits the positive phase shift $\Delta_b + 2\pi \in (0, \pi)$ (cf. Remark 3.10). In contrast, for sufficiently small-amplitude breathers, $\Delta_b \in (-\pi, 0)$ and the phase shift is negative.

Remark 3.14. In the asymptotic limit $k \to 0$ it follows that the background cnoidal wave vanishes, while the bright breather solution recovers the one soliton solution with the spectral paramter $\lambda \in (-\infty, 0)$, while in the asymptotic limit $k \to 1$ the background

cnoidal wave transforms into normalized soliton and the bright breather solution recovers the two-soliton solution with the spectral parameter $\lambda \in (-\infty, -1)$ [28].

3.6 Properties of the dark breather

Figure 3.7 plots Δ_d, κ_d, and c_d for a dark breather as a function of the parameter λ, see Theorem 3.11 and Remark 3.13.

The phase shift Δ_d is monotonically decreasing between the band edges $\lambda_2(k)$ and $\lambda_3(k)$, shown by the vertical dashed lines. The inverse width κ_d has a single maximum and vanishes at the band edges. The breather speed c_d is monotonically decreasing. Since $c_0 = -0.08$ for $k = 0.7$, we confirm that $c_d < c_0$, which is also clear from Figure 3.4. This characterization is in complete agreement with the experimental and numerical findings in [37], in which they observe a dark breather moving slower than a cnoidal carrier wave, while imparting a topological phase shift.

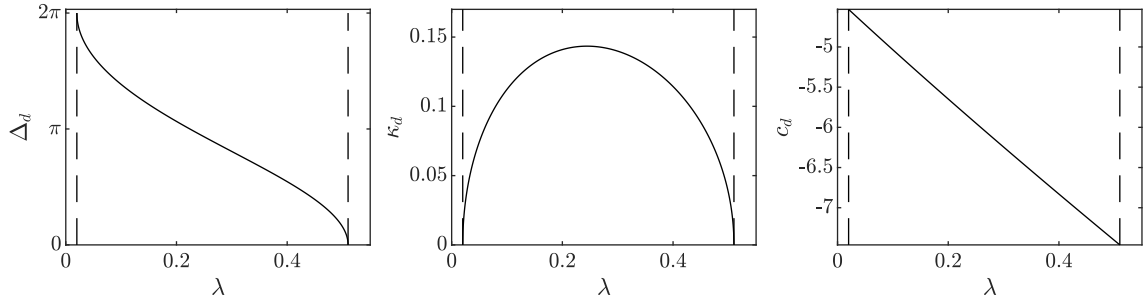

FIGURE 3.7: Normalized phase shift Δ_d (left), inverse width κ_d (middle), and soliton speed c_d (right) versus λ in $(\lambda_2(k), \lambda_3(k))$ for $k = 0.7$. The band edges $\lambda_2(k) = 1 - 2k^2$ and $\lambda_3(k) = 1 - k^2$ are shown by the vertical dashed lines.

Figure 3.8 characterizes the family of dark breathers on a background cnoidal wave by plotting $c_d - c_0$ and κ_d versus Δ_d for three values of k. The profiles of breather solutions at $t = 0$ subject to the phase shift $x_0 = 5$ confirm why we refer to them as dark breathers. In contrast to the bright breather case, dark breather solutions exhibit vanishing cnoidal wave modulations for both of the extreme phase shifts $\Delta_d \to 0$ and $\Delta_d \to 2\pi$, with the largest-amplitude breather occurring at an intermediate phase shift, which we can identify by examining the inverse width κ_d.

Remark 3.15. In the asymptotic limit $k \to 1$ the background cnoidal wave transforms into normalized soliton and the dark breather solution recovers the two-soliton solution with the spectral parameter $\lambda \in (-1, 0)$ [28].

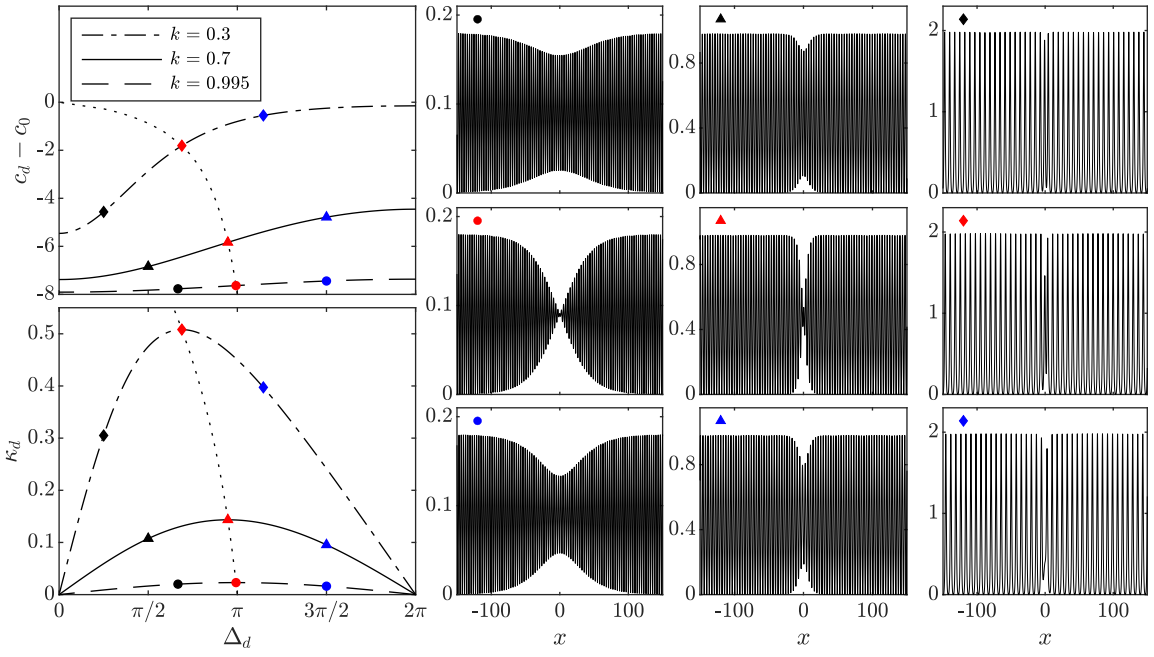

FIGURE 3.8: Left top (bottom): dependence of $c_d - c_0$ (κ_d) versus Δ_d for several values of k. Right: representative solutions for the dark breathers on the background cnoidal wave. Representative solutions are marked on the left panel with a unique colored symbol. The dotted curve on the left panel corresponds to points of maximum κ_d with the greatest localization.

Chapter 4

Concluding Remarks and Open Problems

The two main results of my master's research, on the topic of solitons and dispersive shock waves, are represented in Chapters 2 and 3. In Chapter 2 we considered a physically relevant initial value problem for the KdV equation with the step-like initial data. We show that the step-like initial data evolves into a rarefaction wave (RW) whereas the solitary wave either propagates over the RW or completely disappears inside the RW. This outcome depends on the existence of an isolated eigenvalue of the Schrödinger spectral problem outside the continuous spectrum. One of the main results of this chapter involves construction of the transmitted soliton via the Darboux transformation in the case when an isolated eigenvalue exists. The other important result is the proof that if the isolated eigenvalue does not exist, no embedded eigenvalues exist either, because zeros of the transmission coefficients that correspond to the soliton data transform into complex resonant poles.

In Chapter 3, we have constructed bright and dark breathers on the cnoidal wave background, using the Darboux Transformation. Based on properties of Jacobi elliptic functions, we explored the explicit expressions for parameters of the τ-functions in dependence of the parameter λ to characterize the dynamical properties of the bright and dark breathers. Although the analytical expressions (3.16)-(3.17) and (3.23)-(3.24) are not novel and can be found in equivalent forms in [5, 31, 40], it is the first time to the best of our knowledge that the dynamic properties of the bright and dark breathers have been explicitly investigated.

We hope that this study will open a road for further advances in the subject of solitary wave interactions with the dispersive backgrounds. One of the interesting open problems is to use the Darboux transformation for computations of the limiting phase shifts of the transmitted solitary waves as $t \to \pm\infty$ and comparison with the experimentally detected phase shifts [36, 37]. Another interesting problem is to understand better how the modulation theory for soliton propagation used in our data analysis is justified within the Whitham modulation theory [12, 34, 46]. Although the resolution formulas for N solitons transmitted over the zero background have been derived in [17, 18], it is interesting to see how the transformations between the two problems change these formulas to the case of the nonzero boundary conditions and how these formulas correspond to outcomes of the qualitative theory of soliton tunneling in [43, 44]. Finally, since our approach can be generalized to a larger class of integrable dispersive equations, we hope that this study lays the foundation for exploring other types of dynamic soliton-dispersive background interactions including more complex topological breather structures.

References

[1] M. J. Ablowitz, X. D. Luo, and J. T. Cole, "Solitons, the Korteweg–de Vries equation with step boundary values, and pseudo-embedded eigenvalues", J. Math. Phys. **59** (2018), 091406 (14 pages).

[2] M. J. Ablowitz and H. Segur, *Solitons and the inverse scattering transform* (SIAM, Philadelphia, 1981)

[3] M. J. Ablowitz, *Nonlinear Dispersive Waves: Asymptotic Analysis and Solitons* (Cambridge University Press, Cambridge, 2011)

[4] M. J. Ablowitz, J. T. Cole, G. A. El, M. A. Hoefer, and X. Luo, "Soliton-mean field interaction in Korteweg-de Vries dispersive hydrodynamics," arXiv:221.14884 (2022)

[5] M. Bertola, R. Jenkins, and A. Tovbis, "Partial degeneration of finite gap solutions to the Korteweg–de Vries equation: soliton gas and scattering on elliptic background", arXiv: 2210.01350 (2022)

[6] J. Bernatska, V. Enolski, and A. Nakayashiki, "Sato Grassmannian and Degenerate Sigma Function", Commun. Math. Phys. **374** (2020) 627–660

[7] G. Biondini, S. Li, and D. Mantzavinos, "Soliton trapping, transmission, and wake in modulationally unstable media, Phys. Rev. E **98** (2018) 042211 (8 pages).

[8] G. Biondini, S. Li, and D. Mantzavinos, "Long-time asymptotics for the Focusing nonlinear Schrödinger equation with nonzero boundary conditions in the presence of a discrete spectrum", Commun. Math. Phys. **382** (2021), 1495–1577.

[9] E. D. Belokolos, A. I. Bobenko, V. Z. Enol'skii, A. R. Its, and V. B. Matveev, *Algebro-Geometric Approach to Nonlinear Integrable Equations* (Springer-Verlag, Berlin, 1994)

[10] J. P. Boyd, "Theta Functions, Gaussian Series, and Spatially Periodic Solutions of the Korteweg–de Vries Equation", J. Math. Phys. **23** (1982) 375

[11] P. F. Byrd and M. D. Friedman, *Handbook of Elliptic Integrals for Engineers and Scientists*, 2nd Edition (Springer-Verlag, Berlin, 1971).

[12] W. A. Clarke and R. Marangell, "Rigorous justification of the Whitham modulation theory for equations of NLS type", Stud. Appl. Math. **147** (2021) 577–621

[13] S. Clarke, R. Grimshaw, P. Miller, E. Pelinovsky, and T. Talipova, "On the Generation of Solitons and Breathers in the Modified Korteweg–de Vries Equation", Chaos **10** (2000) 383.

[14] T. Congy, G. A. El, G. Roberti, and A. Tovbis, "Dispersive hydrodynamics of soliton condensates for the Korteweg-de Vries equation," arXiv:2208.04472 (2022)

[15] G. Darboux, "Sur une proposition relative aux équations linéares, Compts Rendus Hebdomadaires des Seances de l'Academie des Sciences, Paris 94 (1882), 1456.

[16] P. Deift and E. Trubowitz, "Inverse scattering on the line," Commun. Pure Appl. Math. **32** (1979) 121–251.

[17] I. Egorova, Z. Gladka, V. Kotlyarov, and G. Teschl, "Long-time asymptotics for the Korteweg–de Vries equation with steplike initial data", Nonlinearity **26** (2013), 1839–1864.

[18] I. Egorova, J. Michor, and G. Teschl, "Soliton asymptotics for the KdV shock waves via classical inverse scattering", arXiv: 2109.08423 (2021).

[19] G. A. El, "Korteweg-de Vries equation: solitons and undular bores", *Solitary waves in fluids*, Adv. Fluid Mech. **47**, 19–53 (WIT Press, Southampton, 2007).

[20] G. A. El and M. A. Hoefer, "Dispersive shock waves and modulation theory", Physica D **333** (2016) 11–65

[21] H. Flaschka, M. G. Forest, and D. W. McLaughlin, "Multiphase averaging and the inverse spectral solution of the Korteweg-de Vries equation," Comm. Pure Appl. Math. **33** (1980) 739–784

[22] C. S. Gardner, J. M. Greene, M. D. Kruskal, and R. M. Miura, "Method for solving the Korteweg-de Vries equation," Phys. Rev. Lett. **19** 1095—1097 (1967).

[23] S. Gavrilyuk and K. M. Shyue, "Singular solutions of the BBM equation: analytical and numerical study", Nonlinearity **35** (2022) 388–410

[24] F. Gesztesy and R. Svirsky, "(m)KdV solitons on the background of quasi-periodic finite-gap solutions", Mem. Amer. Math. Soc. **118** (1995), 563 (88 pages)

[25] M. Girotti, T. Grava, R. Jenkins, K. McLaughlin, and A. Minakov, "Soliton v. the gas: Fredholm determinants, analysis, and the rapid oscillations behind the kinetic equation," arXiv:2205.02601 (2022).

[26] I. S. Gradshteyn and I. M. Ryzhik, *Table of Integrals, Series, and Products* (Academic Press, New York, 2007)

[27] T. Grava and A. Minakov, "On the long-time asymptotic behavior of the modified Korteweg–de Vries equation with step-like initial Data", SIAM J. Math. Anal. **52** (2020), 5892–5993.

[28] M. Hoefer, A. Mucalica and D.E. Pelinovsky, "KdV breathers on a cnoidal wave background", J. Phys. A: Math. Theor. 56 (2023).

[29] X. R. Hu, S. Y. Lou, and Y. Chen, "Explicit solutions from eigenfunction symmetry of the Korteweg–de Vries equation", Phys. Rev. E **85** (2012) 056607

[30] E. L. Ince, *Ordinary Differential Equations* (Dover Publications, New York, 1956)

[31] E. A. Kuznetsov and A. V. Mikhailov, "Stability of stationary waves in nonlinear weakly dispersive media", Sov. Phys. JETP **40** (1974) 855–859

[32] D. F. Lawden, *Elliptic Functions and Applications*, Appl. Math. Sci. **80** (Springer, New York, 1989)

[33] P. D. Lax, "Integrals of nonlinear equations of evolution and solitary waves," Comm. Pure Appl. Math. **21** (1968), 467–490

[34] Y. Liu and D. S. Wang, "Exotic wave patterns in Riemann problem of the high-order Jaulent–Miodek equation: Whitham modulation theory", Stud. Appl. Math. Volume **149** (2022) 588–630

[35] V.B. Matveev and M. A. Salle, *Darboux Transformations and Solitons* (Springer-Verlag, Berlin, 1991).

[36] M. D. Maiden, D. V. Anderson, A. A. Franco, G. A. El, and M. A. Hoefer, "Solitonic dispersive hydrodynamics: Theory and observation," Phys. Rev. Lett. **120** (2018) 144101

[37] Y. Mao, S. Chandramouli, W. Xu, and M. A. Hoefer, "Creation and Interaction of Dark and Bright Topological Breathers from Soliton-Cnoidal Wave Collisions,"ArXiv: 2302.11161, (2023)

[38] Ph. M. Morse and H. Feshbach, *Methods of Theoretical Physics. Volume I* (McGraw–Hill Book Company Inc, New York, 1953).

[39] A. Mucalica and D.E. Pelinovsky, "Solitons on the rarefaction wave background via the Darboux transformation", Proc. R. Soc. A **478** (2022) 20220474 (17 pages)

[40] A. Nakayashiki, "One step degeneration of trigonal curves and mixing of solitons and quasi-periodic solutions of the KP equation", in *Geometric methods in physics XXXVIII* (Birkhäuser/Springer, Cham, 2020), pp. 163–186.

[41] S. P. Novikov, S. V. Manakov, L. P. Pitaevskii and V. E. Zakharov, *Theory of Solitons: The Inverse Scattering Method* (Consultants Bureau, New York, 1984).

[42] B. Oblak, " Orbital Bifurcations and Shoaling of Cnoidal Waves," J. Math. Fluid Mech. **22** (2020) 29

[43] K. van der Sande, G. A. El and M. A. Hoefer, "Dynamic soliton–mean flow interaction with non-convex flux", J. Fluid Mech. **928** (2021) A21 (43 pages).

[44] P. Sprenger, M. A. Hoefer, and G. A. El, "Hydrodynamic optical soliton tunneling", Phys. Rev. E **97** (2018) 032218

[45] H. Van de Vel, "On the Series Expansion Method for Computing Incomplete Elliptic Integrals of the First and Second Kinds", Math. Comp. **23** (1969) 61–69

[46] D. S. Wang, L. Xu, and Z. Xuan, "The complete classification of solutions to the Riemann problem of the defocusing complex modified KdV equation", J. Nonlinear Sci. **32** (2022) 3 (46 pages)

[47] V. E. Zakharov and E. A. Kuznetsov, "Multi-scale expansions in the theory of systems integrable by the inverse scattering transform," Physica D **18** (1986) 455–463

[48] N. J. Zabusky and M. D. Kruskal, "Interaction of "solitons" in a collisionless plasma and the recurrence of initial states", Phys. Rev. Lett. **15** (1965) 240–243.

Appendix A

Jacobi Elliptic Functions

The Jacobi elliptic functions arise from the inversion of the elliptic integral of the first kind,

$$u = F(\varphi, k) = \int_0^{\varphi} \frac{dt}{\sqrt{1 - k^2 \sin^2 t}}$$

where $k \in (0, 1)$ is the elliptic modulus, and $\varphi = am(u, k) = am(u)$ is the Jacobi amplitude. The three basic Jacobi elliptic functions are denoted

$$\mathrm{cn}(u, k) = \cos(\varphi), \quad \mathrm{sn}(u, k) = \sin(\varphi), \quad \text{and} \quad \mathrm{dn}(u, k) = \sqrt{1 - k^2 \sin^2 \varphi},$$

These functions are smooth and periodic, where sn and cn are periodic with period $4K(k)$ while dn is periodic with period $2K(k)$, where $K(k)$ is the complete elliptic integral of the first kind.

The fundamental relations on the Jacobi elliptic functions are given by

$$\mathrm{sn}^2(x, k) + \mathrm{cn}^2(x, k) = 1, \quad \mathrm{dn}^2(x, k) + k^2 \mathrm{sn}^2(x, k) = 1 \tag{A.1}$$

with the following derivative relations

$$\frac{d}{dx} \begin{bmatrix} \mathrm{sn}(x, k) \\ \mathrm{cn}(x, k) \\ \mathrm{dn}(x, k) \end{bmatrix} = \begin{bmatrix} \mathrm{cn}(x, k)\mathrm{dn}(x, k) \\ -\mathrm{sn}(x, k)\mathrm{dn}(x, k) \\ -k^2 \mathrm{sn}(x, k)\mathrm{cn}(x, k) \end{bmatrix}, \tag{A.2}$$

The following table collects together the basic elliptic integrals and functions.

$F(\varphi, k)$	Elliptic integral of the first kind $F(\varphi, k) := \int_0^{\varphi} \frac{d\alpha}{\sqrt{1 - k^2 \sin^2 \alpha}}$
$E(\varphi, k)$	Elliptic integral of the second kind $E(\varphi, k) := \int_0^{\varphi} \sqrt{1 - k^2 \sin^2 \alpha} d\alpha$
$K(k)$	Complete elliptic integral $K(k) := F\left(\frac{\pi}{2}, k\right)$
$E(k)$	Complete elliptic integral $E(k) := E\left(\frac{\pi}{2}, k\right)$
$Z(\varphi, k)$	Zeta function $Z(\varphi, k) := E(\varphi, k) - \frac{E(k)}{K(k)} F(\varphi, k)$
$H(x)$	$\theta_1\left(\frac{\pi x}{2K(k)}\right)$ with $\theta_1(u) = 2\sum_{n=1}^{\infty} (-1)^{n-1} q^{(n-\frac{1}{2})^2} \sin(2n-1)u$
$H_1(x)$	$\theta_2\left(\frac{\pi x}{2K(k)}\right)$ with $\theta_2(u) = 2\sum_{n=1}^{\infty} q^{(n-\frac{1}{2})^2} \cos(2n-1)u$
$\Theta_1(x)$	$\theta_3\left(\frac{\pi x}{2K(k)}\right)$ with $\theta_3(u) = 1 + 2\sum_{n=1}^{\infty} q^{n^2} \cos 2nu$
$\Theta(x)$	$\theta_4\left(\frac{\pi x}{2K(k)}\right)$ with $\theta_4(u) = 1 + 2\sum_{n=1}^{\infty} (-1)^n q^{n^2} \cos 2nu$
q	$e^{-\frac{\pi K'(k)}{K(k)}}$ with $K'(k) = K(k')$ and $k' = \sqrt{1 - k^2}$

TABLE A.1: Table of elliptic integrals and Jacobi elliptic functions.